AGU PUBLICATIONS

Water Resources Research

RESEARCH ARTICLE
10.1002/2013WR014838

Special Section:
Eco-hydrology of Semiarid Environments: Confronting Mathematical Models with Ecosystem Complexity

A modeling approach reveals differences in evapotranspiration and its partitioning in two semiarid ecosystems in Northwest Mexico

Luis A. Méndez-Barroso[1], Enrique R. Vivoni[1,2], Agustin Robles-Morua[1,3], Giuseppe Mascaro[2], Enrico A. Yépez[3], Julio C. Rodríguez[4], Christopher J. Watts[5], Jaime Garatuza-Payán[3], and Juan A. Saíz-Hernández[6]

[1]School of Earth and Space Exploration, Arizona State University, Tempe, Arizona, USA, [2]School of Sustainable Engineering and the Built Environment, Arizona State University, Tempe, Arizona, USA, [3]Departamento de Ciencias del Agua y del Medio Ambiente, Instituto Tecnológico de Sonora, Sonora, Mexico, [4]Departamento de Agricultura y Ganadería, Universidad de Sonora, Sonora, Mexico, [5]Departamento de Física, Universidad de Sonora, Sonora, Mexico, [6]Departamento de Ingeniería Civil y Minas, Universidad de Sonora, Sonora, Mexico

Key Points:
- Simulations with time-varying vegetation greening compare well to field data
- A temporal switch in the dominant component of evapotranspiration was simulated
- Intensive and extensive water use strategies are used in different ecosystems

Correspondence to:
E. R. Vivoni,
vivoni@asu.edu

Citation:
Méndez-Barroso, L. A., E. R. Vivoni, A. Robles-Morua, G. Mascaro, E. A. Yépez, J. C. Rodríguez, C. J. Watts, J. Garatuza-Payán, and J. A. Saíz-Hernández (2014), A modeling approach reveals differences in evapotranspiration and its partitioning in two semiarid ecosystems in Northwest Mexico, *Water Resour. Res.*, *50*, 3229–3252, doi:10.1002/2013WR014838.

Received 3 OCT 2013
Accepted 15 MAR 2014
Accepted article online 8 MAR 2014
Published online 11 APR 2014

Abstract Seasonal vegetation changes during the North American monsoon play a major role in modifying water, energy, and momentum fluxes. Nevertheless, most models parameterize plants as a static component or with averaged seasonal variations that ignore interannual differences and their potential impact on evapotranspiration (*ET*) and its components. Here vegetation parameters derived from remote sensing data were coupled with a hydrologic model at two eddy covariance (EC) sites with observations spanning multiple summers. Sinaloan thornscrub (ST) and Madrean woodland (MW) sites, arranged at intermediate and high elevations along mountain fronts in northwest Mexico, occupy specific niches related to climate conditions and water availability that are poorly understood. We found that simulations with a dynamic representation of vegetation greening tracked well the seasonal evolution of observed *ET* and soil moisture (*SM*). A switch in the dominant component of *ET* from soil evaporation (*E*) to plant transpiration (*T*) was observed for each ecosystem depending on the timing and magnitude of vegetation greening that is directly tied to rainfall characteristics. Differences in vegetation greening at the ST and MW sites lead to a dominance of transpiration at ST ($T/ET = 57\%$), but evaporation-dominant conditions at MW ($T/ET = 19\%$). Peak transpiration occurred at 5 and 20 days after the full canopy development in the ST and MW sites, respectively. These results indicate that evapotranspiration timing and partitioning varies considerably in the two studied ecosystems in accordance with different modes of vegetation greening. Intermediate-elevation ecosystems follow an intensive water use strategy with a rapid and robust transpiration response to water availability. In contrast, higher elevation sites have delayed and attenuated transpiration, suggesting an extensive water use strategy persisting beyond the North American monsoon.

1. Introduction

Vegetation is a key dynamical factor that modifies the water, energy, and momentum fluxes occurring at the land surface [e.g., *Arora*, 2002; *Van den Hurk et al*., 2003; *Vivoni et al*., 2008]. Plant canopies affect the water balance through rainfall interception and plant water uptake during transpiration, while playing a role in the energy balance through radiation attenuation and modifications of surface roughness and albedo [e.g., *Eltahir*, 1998; *Méndez-Barroso and Vivoni*, 2010]. Nevertheless, the impact of vegetation greening on land-atmosphere exchanges is not well understood, in particular during seasonal changes induced by radiation or water availability. This problem is exacerbated when plant transpiration (*T*) is lumped with soil evaporation (*E*) and evaporation of intercepted water (*I*) into a single term, evapotranspiration (*ET*), as this mixes vegetation and soil-mediated processes occurring over disparate temporal and spatial scales. The ability to partition *ET* into its underlying components would improve our understanding of plant water uptake and its feedback to the carbon and water cycle [e.g., *Newman et al*., 2006; *Yépez et al*., 2007]. To date, only a few studies have addressed *ET* partitioning and consensus has not been achieved across different methodologies on the relative importance of each component, even for similar ecosystems [*Reynolds et al*., 2000; *Stannard and Weltz*, 2006; *Scott et al*., 2006; *Moran et al*., 2009; *Raz-Yaseef et al*., 2012; *Yang et al*., 2013].

One approach for estimating *ET* and its components is through the use of models that incorporate vegetation greening either through prognostic equations [e.g., *Kucharik et al*., 2006; *Lawrence et al*., 2007; *Ivanov et al*., 2008] or via remote sensing observations [e.g., *Matsui et al*., 2005; *Cleugh et al*., 2007; *Vivoni*, 2012]. Satellite-derived products, such as the Normalized Difference Vegetation Index (NDVI) and Leaf Area Index (LAI), have been used to provide vegetation parameters for land-atmosphere models instead of the direct simulation of plant processes, at a range of scales from regional to global [*Yan et al*., 2012]. Thus, a first step to include vegetation greening in simulation models has been through comparisons of static and seasonally varying vegetation parameters. *Van den Hurk et al*. [2003], for example, conducted climate simulations to investigate the impact of seasonally varying LAI on evapotranspiration, finding a larger range of values due to increases in summer *ET* and decreases in winter *ET*, as compared to static conditions. Furthermore, *Tang et al*. [2012] showed that the interannual variability of seasonal (summer) changes in LAI were important to account for when predicting spatiotemporal patterns of evapotranspiration using a hydrologic model, in particular during periods of vegetation green-up. While promising, open questions remain with respect to the seasonal and interannual variations of *ET* and its components and how these are linked to readily available information about an ecosystem, such as precipitation or vegetation greening. Furthermore, few studies have accounted for the complete set of changes to plant processes (e.g., radiation, interception, transpiration) that simultaneously occur during vegetation greening.

In a recent study, *Vivoni* [2012] conducted hydrologic simulations using the Triangulated Irregular Network (TIN)-based Real-time Integrated Basin Simulator (tRIBS) [*Ivanov et al*., 2004; *Vivoni et al*., 2007a] that accounted for seasonal variations in vegetation parameters. The study was focused on an intermediate-sized watershed ($\sim$100 km^2) experiencing dramatic vegetation greening during the North American monsoon (NAM). The NAM is a summertime atmospheric circulation occurring in the southwestern U.S. and northwestern Mexico that leads to increased precipitation, soil moisture, evapotranspiration, and streamflow in the arid and semiarid area. A large number and variety of ecosystems respond to the rainy season through biomass production, leading to regional patterns in vegetation greenness [*Watts et al*., 2007; *Méndez-Barroso et al*., 2009; *Lizárraga-Celaya et al*., 2010; *Forzieri et al*., 2011]. *Vivoni* [2012] found that ecosystem-specific variations in vegetation greening were responsible for the simulated spatiotemporal patterns of *ET* components. For example, subtropical scrubland ecosystems, such as Sinaloan thornscrub (ST), exhibited early greening in the summer season that favored high plant transpiration, whereas oak savanna ecosystems, such as Madrean woodland (MW), had a more delayed and prolonged green-up with sustained plant transpiration into the early fall. However, the focus of *Vivoni* [2012] on a single summer did not permit an assessment of the interannual variations in evapotranspiration and its partitioning or on the differences among ecosystems.

In this study, we seek to understand how variations in vegetation greening affect *ET* partitioning in two semiarid ecosystems (ST and MW) in northwestern Mexico. By virtue of their organization along semiarid mountain fronts, these ecosystems occupy specific niches related to climate conditions and water availability that also likely occur in other semiarid regions. To do so, we utilize the tRIBS model applied to an eddy covariance tower site in each ecosystem, while accounting for the impact of seasonal greening on the vegetation parameters in the model. For the first time, this approach allows a direct comparison between the ST and MW ecosystems, arranged from intermediate ($\sim$600 to 1200 m for ST) to high ($\sim$1200 to 1700 m for MW) elevations, in terms of both observations and simulations. Based on data availability, multiple summer periods are studied in each ecosystem to cover a range of seasonal precipitation amounts. We are interested in answering the following questions that are broadly applicable to other ecosystems: How do seasonal variations in vegetation greening in the different ecosystems affect *ET* partitioning? and Do interannual differences in rainfall and vegetation greening affect *ET* and its components? While we focus primarily on *ET*, the surface soil moisture and sensible heat flux are also inspected due to its importance in controlling *ET* rates or serving as a complementary measure of the surface energy balance.

2. Methods

2.1. Study Region

The study region is located in northern Sonora, Mexico, in a rural, sparsely populated area characterized by north to south trending mountain ranges and valleys that are part of the Sierra Madre Occidental.

Table 1. Mean Monthly Precipitation and ±1 Monthly Standard Deviation (sd) and Summer Season (JJAS) Precipitation at Sinaloan Thornscrub and Madrean Woodland Sites Over 2004–2009

	Mean (±1 sd) Precipitation (mm)	
Month or Year	Sinaloan Thornscrub	Madrean Woodland
Jun	28 (±27)	39 (±21)
Jul	169 (±38)	180 (±113)
Aug	165 (±61)	177 (±59)
Sep	84 (±88)	41 (±12)
2004	278	
2006	549	
2007	490	
2008	519	551
2009	397	321

Ecosystems in the region vary from desert shrublands to conifer pine forests, with a significant proportion of subtropical species [*Méndez-Barroso and Vivoni*, 2010]. Overall, site climate is considered steppe or semiarid (BSh), according to the Köppen-Geiger classification [*Peel et al*., 2007], characterized by hot, arid conditions, and winter temperatures above 0°C. The two study sites are located in the Río San Miguel basin (3796 km^2), which have mean annual precipitation values (±1 standard deviation) ranging from 481 ± 181 mm/yr (Rayón, near ST) to 496 ± 204 mm/yr (Meresichic, near MW), over 1981–2006. Table 1 presents the site-specific monthly and summer seasonal precipitation values over the periods with available data. Mean annual air temperatures in the region range from 21.4 ± 6.4°C (Rayón, near ST) to 18.9 ± 6.1°C (Meresichic, near MW), over 1981–2006. The Sinaloan thornscrub (ST) site is located on top of an alluvial foothill near Rayón (29.74°N, 110.54°W) at an elevation of 632 m, while the Madrean woodland (MW) site is found on a gentle mountain slope, ~21 km southeast of Meresichic (29.96°N, 110.46°W) at an elevation of 1314 m. Figure 1 depicts the location of the study region and the elevation and ecosystem characteristics of the two sites. Transects A-A′ and B-B′ clearly show how the sites represent intermediate and high elevations along these semiarid mountain fronts [cf., *Vivoni et al*., 2007b, 2010]. All ecosystems in the region respond by greening to the seasonal precipitation from the NAM extending from July to September and leading to 60–70% of the annual precipitation [*Méndez-Barroso et al*., 2009].

2.2. Field and Remote Sensing Observations

An eddy covariance (EC) tower was deployed at each site in an area of homogeneous vegetation cover within the EC fetch to measure water, energy, and carbon fluxes, as well as site meteorology, during the summer season (1 June to 30 September) over multiple years. Figure 2 provides details of the characteristics of each site, including a high-resolution (~1 m) terrain model obtained using site surveying and a 1 m satellite image depicting the vegetation patterns. The ST site was installed in 2004 as part of the SMEX04 (Soil

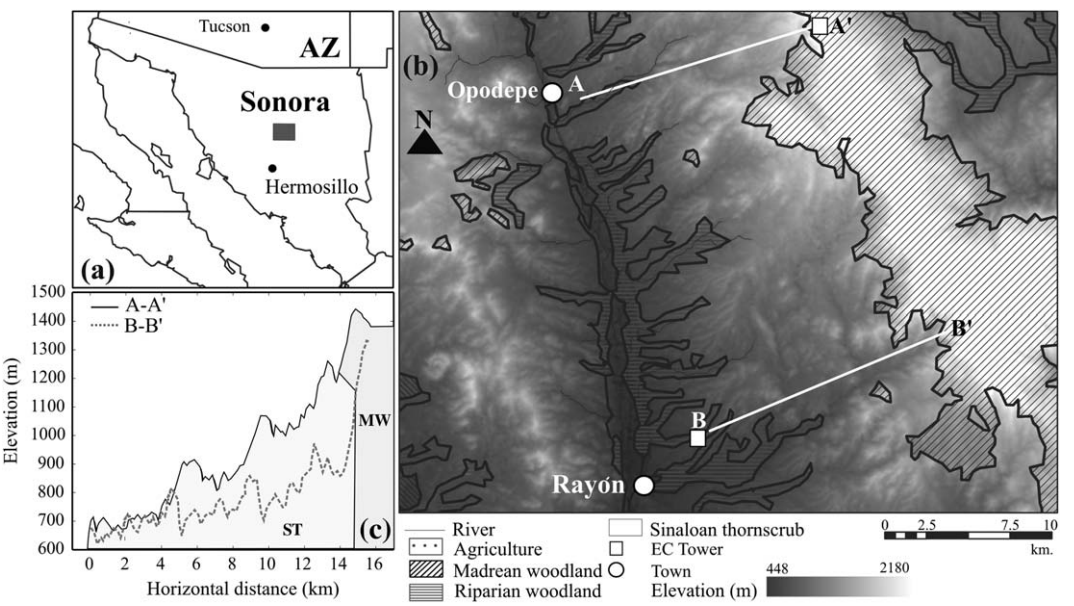

Figure 1. (a) Location of the study site in Sonora, Mexico. (b) Location of two eddy covariance (EC) tower sites and their relation to ecosystem and topographic distributions in the region. Note that the Sinaloan thornscrub is represented as transparent. MW is at A′ and ST is at B (square symbols). (c) Elevation cross sections along the mountain fronts containing the two EC sites with extents of ST and MW ecosystems labeled.

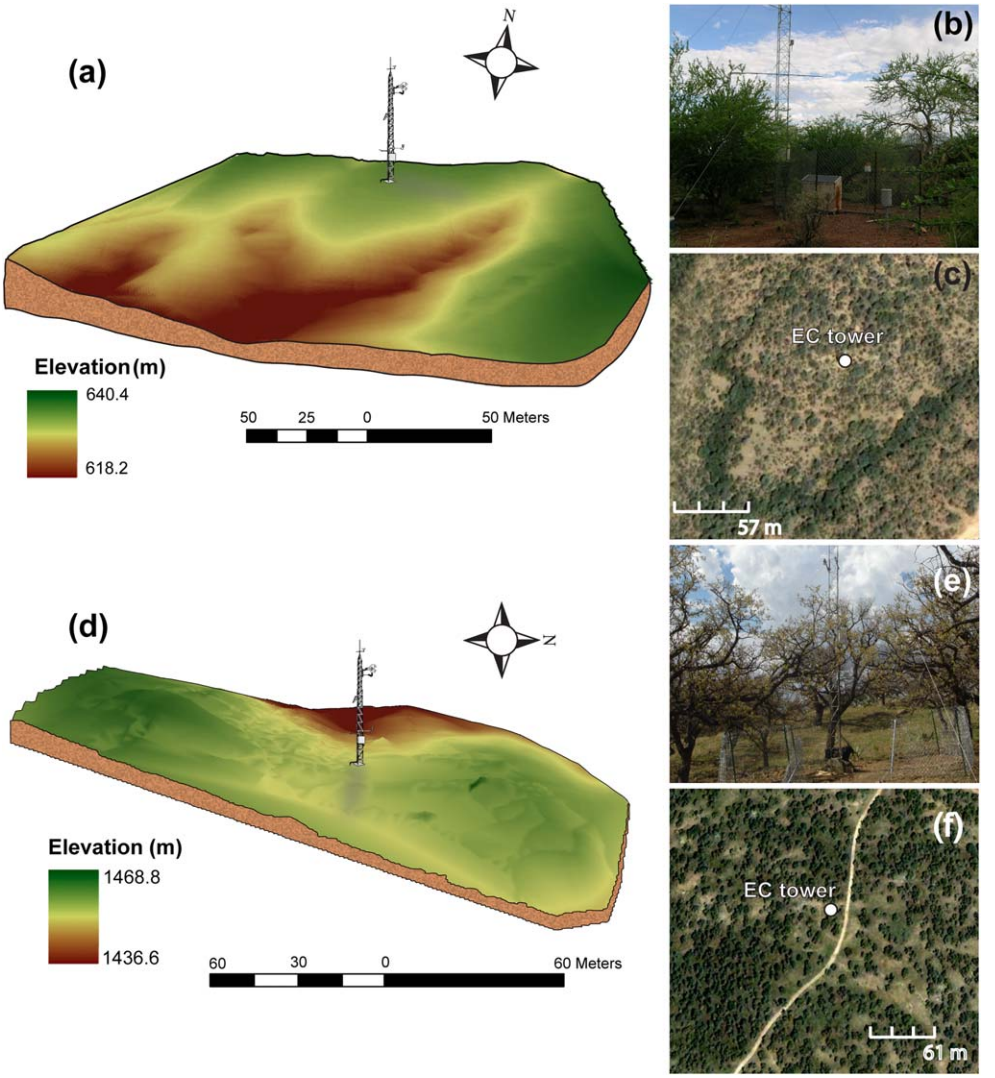

Figure 2. Topographic and vegetation characteristics at EC tower sites. (a) Topographic survey, (b) tower photograph, and (c) 1 m IKONOS image at the Sinaloan thornscrub site near Rayón, Sonora. (d) Topographic survey, (e) tower photograph, and (f) 1 m IKONOS image at the Madrean woodland, 16.6 km northeast of Opodepe, Sonora.

Moisture Experiment 2004) experiment [*Bindlish et al*., 2008] and was operated for summers 2006–2009 as part of this study for five summers of observations. Vegetation at the ST site includes thorny, deciduous trees, and shrubs, as well as cacti and succulents, with low amounts of grass cover [see *Brown*, 1994, for a description of ST]. *Watts et al*. [2007], *Méndez-Barroso and Vivoni* [2010], *Vivoni et al*. [2010], *Tang et al*. [2012], and *Tarín et al*. [2014] have reported on the EC data at the ST site. On the other hand, the MW site was installed in 2007 and operated in 2008 and 2009 allowing for only two summers (as with ST, the EC system continues to be operated during short periods). Vegetation at the MW site is primarily oak trees interspersed with grasses and succulents [*Brown*, 1994]. To date, the EC data at the MW site have not been reported on, though *Méndez-Barroso et al*. [2009] described the precipitation, soil moisture, and vegetation at a nearby site, and detailed simulations have not been conducted at the site. Both the ST and MW EC systems form part of a growing network of flux measurements in Mexico [*Vargas et al*., 2013]. Figure 3 shows the seasonal evolution of rainfall and surface soil moisture (*SM*, top 10 cm) for the 2004–2009 summers in the ST and MW sites as bi-weekly averages and ± 1 standard deviations.

Both EC systems have a standard configuration consisting of a three-dimensional, sonic anemometer (CSAT3, Campbell Scientific, Logan, UT) and an open-path Infrared Gas Analyzer (LI7500, LI-COR, Lincoln, NE) aligned to the dominant wind direction of 225° [*Moncrieff et al*., 2000]. EC sensors were placed at 9 m

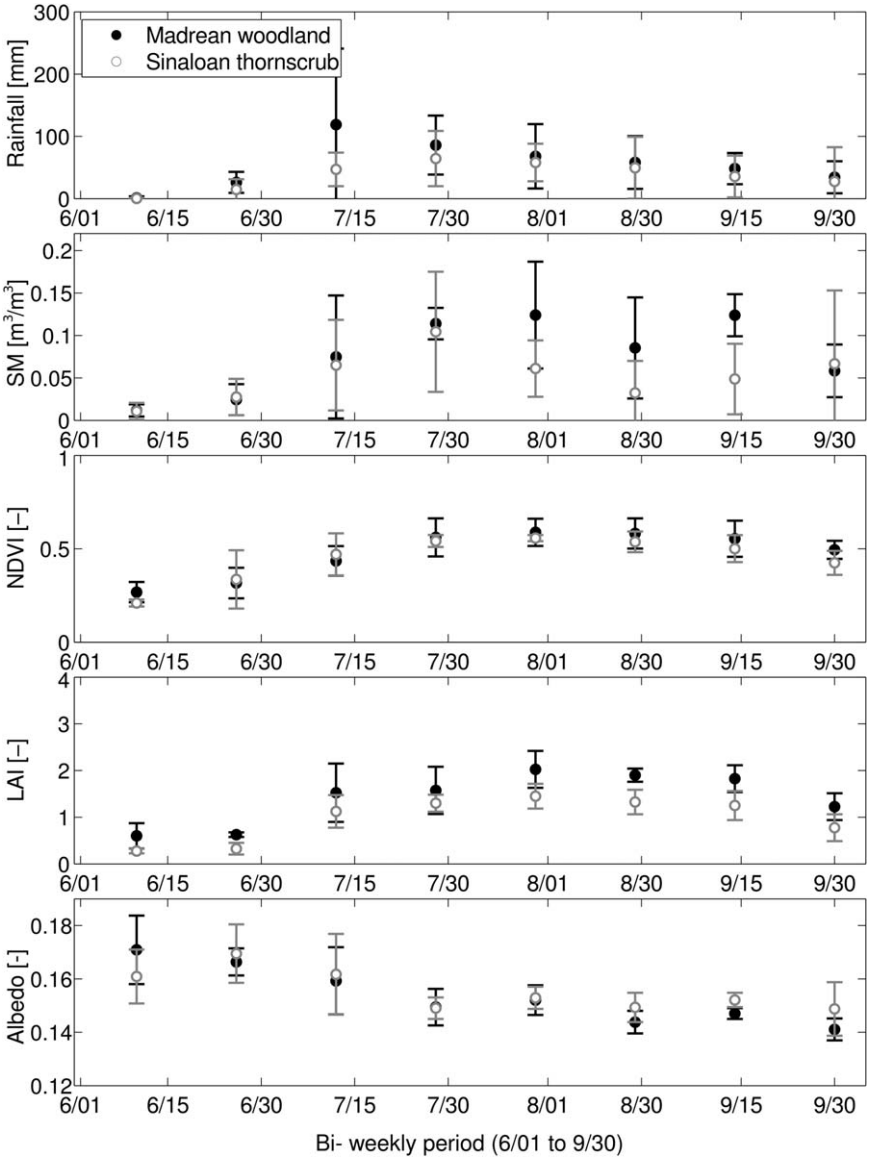

Figure 3. Seasonal evolution of rainfall, surface soil moisture (*SM*, top 10 cm), Normalized Difference Vegetation Index (NDVI), Leaf Area Index (LAI) and albedo over 2004–2009. Rainfall is accumulated during biweekly intervals, while *SM* is averaged over this period. NDVI, LAI, and albedo represent 16 day composites from MODIS. Symbols depict biweekly averages and error bars are ±1 standard deviations across all years.

above ground (installed at 2 m above the canopies). Net shortwave and longwave radiation were measured (CNR2, Kipp and Zonen, Delft, Netherlands), along with incoming solar radiation (CMP3, Campbell Scientific). Ground heat flux was measured using two soil plates (HFP01SC, Hukseflux, Manorville, NY) placed at 2 cm depth. Site rainfall was measured using a tipping-bucket rain gauge (TB3, Hydrological Services, Sydney, Australia at ST and TR-52USW, Texas Electronic, Dallas, TX at MW), while soil moisture was measured using soil dielectric sensors (Stevens Hydra sensor, Portland, OR) at each site at 5 and 10 cm depths, with MW having additional sensors at 15 and 30 cm. We used here the 5 and 10 cm depth soil moisture sensors due to their greater data availability at both sites. It should be noted that the soil moisture response at MW beyond 10 cm was similar to the shallower sensors (not shown). Sensors were connected to CR5000 dataloggers (Campbell Scientific) with the EC sensors operating at 20 Hz and averaging data to 30 min periods. Covariances of vertical wind speed, temperature, and water vapor concentration were processed to obtain the sensible (H) and latent heat (λE) flux using EdiRe (University of Edinburgh). Turbulent flux corrections for the EC measurements followed *Scott et al*. [2004] and included data filtering (i.e., data removal after or during

rain events and outliers), the Webb method for density correction [*Webb et al*., 1980], the quality check method described by *Mauder and Foken* [2004] and the planar fit as a method of rotation [*Wilczak et al*., 2001]. The planar fit method is deemed appropriate for correcting EC measurements for nonzero mean vertical velocity in the sloping terrain at both sites [*Lee et al*., 2004], but more markedly at MW (Figure 2). Ground heat flux (G) was corrected for heat storage in the upper 2 cm using the change in soil temperature measured by two thermocouples at 2 cm depth (TCAV-L, Campbell Scientific) and the volumetric water content at 5 cm depth [*Campbell Scientific, Inc*., 2012]. The soil temperature readings from the thermocouples were averaged and then used to calculate the soil heat storage and compute the corrected ground heat flux. Canopy heat storage is expected to be small in short vegetation types (less than 8 m) and was neglected in this study [*Wilson et al*., 2002].

Energy balance closure was evaluated for each site using a least squares comparison between turbulent fluxes ($\lambda E + H$) and available energy ($R_n - G$, where R_n is net radiation) and the seasonal energy balance ratio (ENR, defined as the cumulative sums of turbulent fluxes divided by the available energy) obtained for all available summers. The ST site had a slope of 0.75 ($\pm$0.04), an intercept of 16 ($\pm$2) W/m^2, a correlation coefficient (r^2) of 0.93 ($\pm$0.005) and an ENR of 0.83 ($\pm$0.02), while the MW site had a slope of 0.81 ($\pm$0.05), an intercept of 27 ($\pm$18) W/m^2, a correlation coefficient (r^2) of 0.90 ($\pm$0.06) and an ENR of 0.81 ($\pm$0.10), where the errors are computed as interannual standard deviations among the summers. Reported values for MW were affected by a net radiometer malfunction in June 2009, after which a replacement sensor led to a large improvement in the energy balance closure (i.e., increase in the slope from 0.60 to 0.81). These metrics are close to values reported by *Wilson et al*. [2002] for the energy balance closure at FLUXNET sites and as such we opted not to correct the EC turbulent flux measurements to account for ENR in these heterogeneous and open canopies that are subject to larger systematic errors [*Baldocchi et al*., 2000; *Kustas et al*., 2000]. To validate the simulated fraction of plant transpiration to evapotranspiration (T/ET), we used a field data set of T/ET obtained through the stable isotope method described by *Yépez et al*. [2003]. These daily integrated values of T/ET were sampled during 24–27 July 2007, and 15–16 July, 2008, by *Tarín et al*. [2014] in the subtropical scrubland. These 4 days exhibited relatively small measurement errors due to the wet soil conditions experienced at the site from recent storms.

We complemented the field observations with an analysis of remote sensing data on vegetation greening using the MODerate resolution Imaging Spectroradiometer (MODIS) sensors on board the EOS Terra and Aqua satellites, following *Méndez-Barroso et al*. [2009] and *Lizárraga-Celaya et al*. [2010]. One of the limitations of remote sensing data in the visible and near infrared regions is the presence of cloud cover during the NAM. To overcome this, we used composite products: 16 day composites of NDVI (MOD13Q1, 250 m spatial resolution) and white-sky shortwave albedo (MOD43B, 1 km), along with 8 day composites of LAI and fraction of Photosynthetically Active Radiation (fPAR, MOD15A2, 1 km). We spatially averaged the 250 m NDVI data to 1 km to match the resolution of the other products. NDVI, fPAR, and LAI from MODIS have been shown to represent vegetation conditions well in semiarid regions as compared to ground measurements [*Privette et al*., 2002; *Fensholt et al*., 2004; *Ryu et al*., 2012]. Figure 3 illustrates the seasonal evolution of NDVI, albedo and LAI for summer periods at the ST and MW sites as biweekly averages and $\pm$1 standard deviations. Data sets spanned from 1 June to 30 September over 2004 to 2009 and included the extraction of the 1 km area around each EC tower using the MODIS Data Subsetting and Visualization Tool. Composites were linearly interpolated to daily values to allow for a gradual progression of vegetation changes. In addition, a smoothing technique that included the combination of weighted local regression and a second-degree polynomial model (with a span of 5%) was applied to the raw data to eliminate noise. This also accounts for the uncertainty in the timing of measured values within the composite. The resulting time series of NDVI, LAI, fPAR, and albedo at the ST and MW sites constituted the basis for deriving vegetation parameters used in the modeling efforts described next.

2.3. Hydrologic Model and its Application

Hydrologic simulations were performed using the tRIBS model applied to the ST and MW sites independently. A single, hexagonal Voronoi polygon (or model element) was generated from a 30 m Digital Elevation Model (DEM) derived from the Advance Space-borne Thermal Emission and Reflection Radiometer (ASTER). A model element with an area of 98.77 m^2, a soil depth of 1 m (based on a soil pit dug at each site) and a gentle slope was used at each location. In this study, tRIBS is used as a one-dimensional model to simulate hydrologic processes that track the response to meteorological forcing, including: (1) rainfall interception, (2) evaporation from bare soil (E) and intercepted water (I) and plant transpiration (T), (3) infiltration and

Table 2. Soil Parameters Used in the Simulations[a]

Parameter	Variable (Unit)	Sinaloan Thornscrub	Madrean Woodland
Saturated hydraulic conductivity	K_s (mm/h)	55	30
Soil moisture at saturation	θ_s	0.41	0.45
Residual soil moisture	θ_r	0.02	0.04
Pore distribution index	m	0.85	0.50
Conductivity decay parameter	f (mm^{-1})	0.0001	0.0010
Porosity	n	0.45	0.48
Volumetric heat conductivity	k_s (J/ms K)	0.20	0.20
Soil heat capacity	C_s (J/m^3 K)	1.61×10^6	1.47×10^6

[a]For the Sinaloan thornscrub, values were based on *Vivoni et al*. [2010] with minor adjustment to K_s. For the Madrean woodland, K_s, θ_s, and n were estimated using the pedotransfer functions of *Rawls et al*. [1983] using soil texture data; θ_r was obtained from *Van Genuchten* [1980]; m was estimated according to *Rawls and Brakensiek* [1989]; f was based on the logarithmic relation between K_s with soil depth following *Robles-Morua et al*. [2012]; and k_s and C_s were determined from *Lapham* [1989].

moisture redistribution, and (4) runoff production. Appendix A details the evapotranspiration calculations in tRIBS and how *ET* is partitioned into *E*, *T*, and *I*. *Ivanov et al*. [2004] provides a description of infiltration into the sloped, heterogeneous soil above an impermeable layer. Single infiltration fronts interact with a pre-storm moisture profile, determined from hydrostatic equilibrium, and the water table position. This interaction leads to a range of possible soil moisture states, which influence infiltration and runoff generation via infiltration-excess, saturation-excess, perched return flow and groundwater exfiltration mechanisms.

Meteorological forcings to the hydrologic model were obtained from measurements at each site over the study periods (1 June to 30 September at 30 min time step). The month of May was also included in each year (2004, 2006–2009 at ST and 2008–2009 at MW) to allow for an initial drying period that helped reduce soil moisture to low values near the residual level (θ_r) prior to the onset of the NAM. This initialization is possible due to the annual resetting of the soil moisture conditions during the dry spring prior to the summer rainy season [*Vivoni et al*., 2010]. Model forcings consisted of precipitation (mm), atmospheric pressure (Pa), relative humidity (%), wind speed (m/s), air temperature (°C), and incoming solar radiation (W/m^2) with a time resolution of 30 min. Gaps in the meteorological observations due to periods of no data collection were filled in with ground-adjusted forcing from the North American Land Data Assimilation System (NLDAS) [*Mitchell et al*., 2004], following *Robles-Morua et al*. [2012]. The percentage of time with gap-filled forcing ranged from 13% to 67% of the periods, depending on the site and year, with the largest gaps for 2006–2007 (ST, 61% and 67%) and 2008 (MW, 63%).

Soil parameters were obtained through a manual calibration process that focused on the 2006 and 2008 summer periods for ST and MW sites, respectively. In this process, the soil parameters remained constant in time for each site. Initial parameter values were obtained from soil pedotransfer functions based on particle size fraction and bulk density [*Van Genuchten*, 1980; *Rawls et al*., 1983; *Rawls and Brakensiek*, 1989; *Lapham*, 1989]. At the ST site, soil analyses indicated a sandy loam texture in the top 30 cm and sandy clay in the lower profile down to about 75 cm. At the MW site, soil analyses revealed a sandy loam texture in the upper 40 cm of soil and a sandy clay loam down to the 55 cm of sampling depth. Manual adjustments to soil parameters within feasible ranges were performed independently at each site for the calibration periods only, based on the comparison of observed and simulated surface soil moisture (*SM*, top 10 cm) and evapotranspiration (*ET*) using the Mean Absolute Error (MAE), Correlation Coefficient (CC), and Bias (B, see Appendix B). Sensible heat flux (*H*) was inspected for model validation purposes only using similar metrics, while root zone soil moisture (top 1 m) was not used in the model calibration or testing due to a lack of similar observations. Table 2 presents the soil parameters for each site and their source. Note the manual procedure allowed us to retain well-constrained values from pedotransfer functions, while focusing on parameters with higher uncertainty, such as the pore distribution index. Model testing was then performed for the remaining summer periods (2004, 2007–2009 at ST and 2009 at MW).

Vegetation parameters were specified as time-varying quantities based on relationships to remotely sensed data from MODIS. Appendix C describes the empirical equations used to transform the linearly interpolated, daily MODIS observations of LAI, NDVI, fPAR, and albedo into the vegetation parameters defined in Table 3. The implemented relations are considered more sophisticated than the methods presented by *Vivoni* [2012], in particular with respect to *S*, *p*, and r_s. Three scenarios were considered to examine the effects of

Table 3. Vegetation Parameters at the Sinaloan Thornscrub and Madrean Woodland Sites for the Three Simulation Scenarios[a]

		Sinaloan Thornscrub			Madrean Woodland		
Parameter	Variable (Unit)	Dynamic	Leaf Off	Leaf On	Dynamic	Leaf Off	Leaf On
Free throughfall coefficient	p	0.09–0.78	0.75	0.13	0.06–0.51	0.51	0.06
Maximum canopy storage	S (mm)	0.07–0.75	0.09	0.67	0.23–0.94	0.23	0.97
Albedo	a	0.13–0.19	0.18	0.15	0.13–0.17	0.17	0.14
Vegetation height	h (m)	6	6	6	8	8	8
Optical transmission coefficient	k_t	0.37–0.90	0.89	0.42	0.55–0.86	0.86	0.55
Minimum canopy stomatal resistance	r_s (s/m)	19.5–247	197	23	18–94	85	18
Vegetation fraction	v_f	0–0.95	0.00	0.76	0–0.68	0.00	0.61
Soil evaporation stress factor	β_E	0.55	0.55	0.55	0.55	0.55	0.55
Plant transpiration stress factor	β_T	0.10	0.10	0.10	0.55	0.55	0.55

[a]Constant β_E and β_T were obtained from model calibration. For the Dynamic scenario, parameter ranges shown represent minimum and maximum values.

vegetation greening on the simulated *ET* and *SM*: (1) Dynamic (time-varying plant parameters for each year), (2) Leaf off (fixed or time-constant vegetation parameters with no leaves), and (3) Leaf on (fixed vegetation parameters under full canopy conditions). For each scenario, the vegetation parameters apply to the vegetation fraction or green cover (v_f) of the model element occupied by a subtropical tree species at ST and an oak tree at the MW site, while the $1 - v_f$ fraction is treated as bare soil. Note that the green vegetation fraction of a model element varies from near zero (Leaf off) to values near 0.7 or 1 (Dynamic) in Table 3. To obtain the Leaf off values, the mean of the minimum values of v_f and S were calculated for each site over the 2004–2009 period, while the mean of the maximum values of a, k_t, p, and r_s where utilized to represent dormancy. In contrast, Leaf on conditions were based on the mean of the maximum v_f and S and the mean of the minimum a, k_t, p, and r_s over 2004–2009. This selection implies that Leaf off and Leaf on scenarios are representative of average minimum and maximum greenness over five summers. As a result, care must be taken when interpreting results from each summer at each site relative to this selection. Note that the Dynamic scenario varies for each summer, thus effectively capturing interannual variations in vegetation greening and its impact on all correlated plant processes.

Evapotranspiration partitioning depends on the ability of *E* and *T* to extract soil water from the surface and root zones, respectively [e.g., *Newman et al.*, 2006]. In the model, this is parameterized using piecewise linear relations between *E* and surface soil moisture (top 10 cm) and *T* and root zone soil moisture (top 1 m), which are controlled by stress factors (Appendix A) [*Ivanov et al.*, 2004]. The selection of the soil evaporation (β_E) and plant transpiration (β_T) stress factors (Table 3) was based on a manual parameter sensitivity analysis for the calibration periods in each ecosystem, as opposed to the fixed and equal factors used by *Vivoni* [2012]. The sensitivity analysis systematically varied β_E and β_T within the 0–1 range to explore all possible combinations at each site. We selected the pair of β_E and β_T that minimized the simulated errors in *ET* and *SM* with respect to the observations at each site using the MAE, CC, and B metrics. The resulting values indicate that soil evaporation stress factors are similar in each ecosystem ($\beta_E = 0.55$) which is consistent with the sandy loam texture at each site. The plant transpiration stress factor, on the other hand, varied with plant functional type with β_T having smaller values at ST ($\beta_T = 0.1$), as compared to MW ($\beta_T = 0.55$), due to the greater capacity of ST to sustain plant *T* under lower soil moisture conditions [*Vivoni et al.*, 2008]. This is also consistent with the more rapid green-up in the subtropical scrubland, which suggests a more efficient use of soil water by transpiration [*Méndez-Barroso et al.*, 2009; *Forzieri et al.*, 2011].

3. Results

3.1. Seasonal Evolution of Vegetation Parameters

Figure 4 depicts the seasonal evolution of the vegetation parameters averaged over all simulation periods, including ± 1 standard deviations to represent interannual variability. Clearly, the onset of vegetation greening in early July leads to large changes in the representation of vegetation parameters in the model. For example, the vegetation fraction (v_f) increases from values near zero to an average of 0.6 in the subtropical scrubland and 0.5 in the oak savanna. The interannual variability in v_f is higher at the MW site, in particular near the peak values. Overall, note that the ST site typically has earlier maximum or minimum values in vegetation parameters (mid-July) as compared to MW (mid-August). Since vegetation parameters were derived

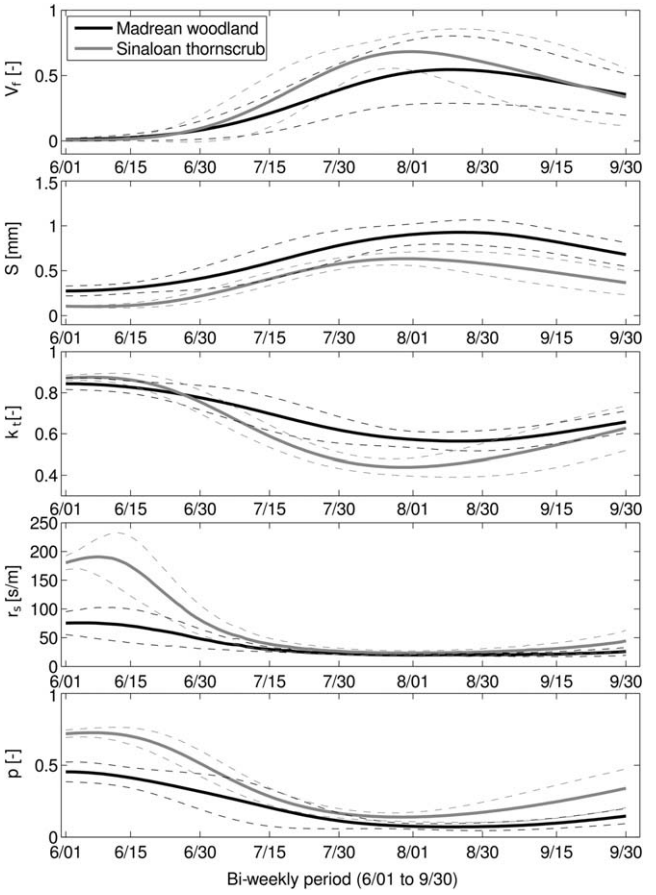

Figure 4. Seasonal evolution of vegetation parameters from MODIS for the Sinaloan thornscrub (gray solid line, 2004, 2006–2009) and Madrean woodland (black solid line, 2008–2009) sites. Dashed lines depict ±1 standard deviation in time for each ecosystem across all summers. Vegetation parameters were estimated based on empirical relations that link vegetation fraction (v_f), maximum canopy storage (S), optical transmission coefficient (k_t), minimum canopy stomatal resistance (r_s), and free throughfall coefficient (p) with Leaf Area Index (LAI), fraction of photosynthetically active radiation (fPAR), and Normalized Difference Vegetation Index (NDVI).

from remote sensing data, these all exhibit internally consistent temporal variations. Furthermore, differences between the two sites are consistent with field evidence [*Vivoni et al*., 2010; *Tarín et al*., 2014], indicating that ST has a higher vegetation cover (higher v_f) and shading (lower k_t), but a lower interception capacity (lower S and higher p). Overall, the time-varying v_f is a major difference between the ecosystems since it has a strong control on *ET* partitioning [*Vivoni*, 2012]. Furthermore, the fraction $1 - v_f$ is considered in the model as bare soil in both ecosystems, where grasses and forbs, cacti, or succulents may actually occupy these understory spaces.

3.2. Seasonal and Interannual Variations in *ET* and *SM*

The multiple summer periods at the ST and MW sites allow for a comparison of the seasonal evolution of *ET* and *SM* for varying interannual conditions. As shown in Table 1, total summer precipitation (JJAS) can vary substantially in the region, in accordance with the strength of the NAM [*Higgins and Shi*, 2001; *Gutzler*, 2004; *Forzieri et al*., 2011]. As compared to long-term averages at Rayón (near ST site) and Meresichic (near MW site but at lower elevation), the study periods fall into below-average (2004 and 2009) and average (2006–2008) categories. Soil moisture, vegetation greenness, and evapotranspiration are expected to vary in response to year-to-year differences in precipitation [e.g., *Tang et al*., 2012]. Furthermore, the onset and demise of the NAM varies interannually, leading to changes in the timing and duration of greening and its associated effects on water and energy fluxes. As such, we first present the comparison of model simulations that capture vegetation seasonality in each summer to the observations in each site. For reference, the smoothed, daily NDVI time series is presented along with the composite NDVI values placed at the midpoint of the compositing period.

Figure 5 presents the seasonal evolution and interannual differences in observed rainfall, vegetation greening (NDVI), and surface soil moisture (average of top 10 cm of soil) as derived from available observations (average of sensors at 5 and 10 cm) and model simulations using the Dynamic scenario at the ST site. Note how precipitation pulses affect the rapid vegetation green-up and their coincident influence on the surface soil moisture. Diurnal fluctuations are due to a temperature-dependence of the sensors when installed at shallow depths [*Seyfried and Murdock*, 2004; *Vivoni et al*., 2007b] and not a diurnal redistribution of soil moisture. The observed and simulated soil moisture (depicted volumetrically as m^3/m^3 at 30 min intervals) match well, in particular with respect to average conditions and the peak and recession characteristics of each wetting event across all summers. Model performance was inferior during periods when: (1) meteorological forcings from the tower were missing and NLDAS products were used in their place (i.e., 2006 had a

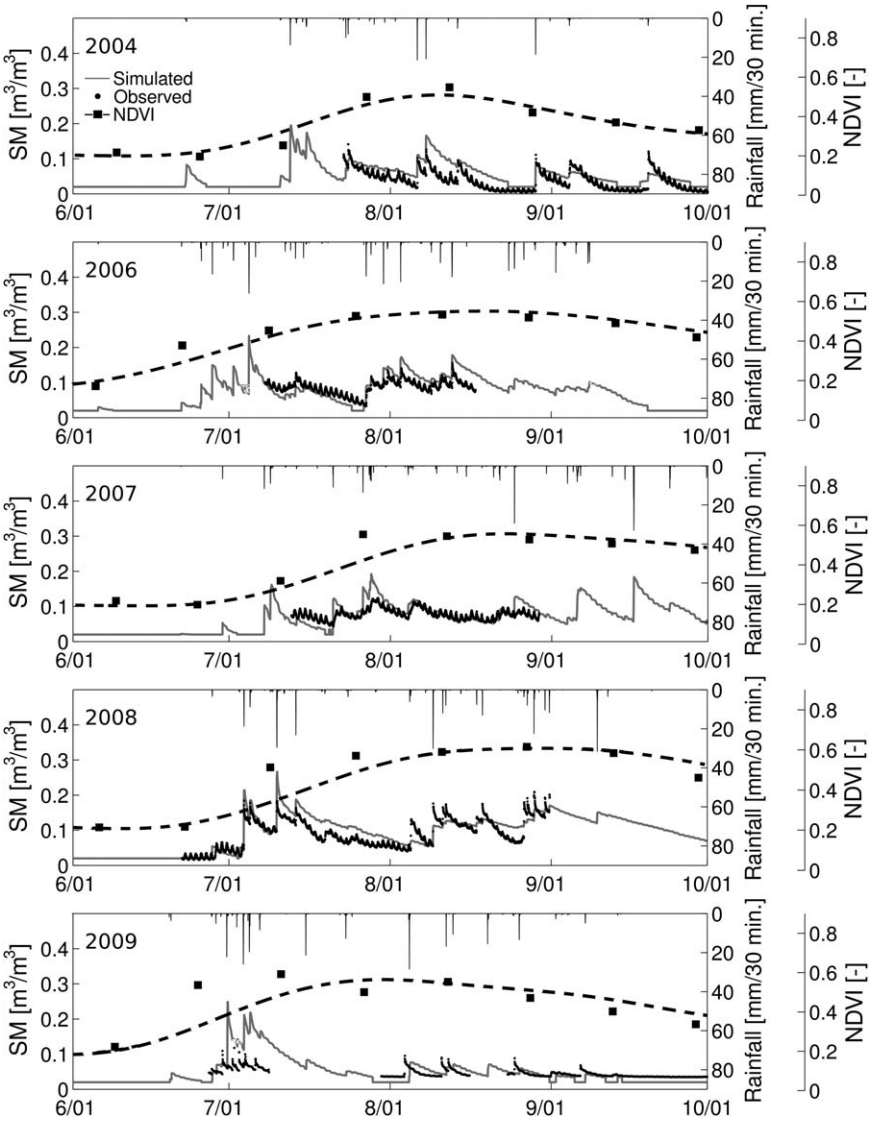

Figure 5. Comparison of observed and simulated soil moisture (*SM* at 10 cm depth) at the Sinaloan thornscrub site for 2004 and 2006–2009. Model simulations account for the Dynamic scenario. For reference, NDVI shows the vegetation greenness variations at the site with the squares indicating the composite data with the smoothed series as dashed lines. Gaps in the observations due to sampling protocols or equipment malfunction are depicted by missing data.

high percentage of missing tower forcing, 67%), and (2) soil moisture sensors did not operate correctly (i.e., 2009 had issues with soil moisture data availability and quality). Note that the same soil parameters (Table 2) were used for each summer based on the calibration period, such that only meteorological forcing and vegetation parameters vary in time each summer in accordance with the observed conditions. Table 4 provides a quantitative evaluation of *SM* at the 30 min resolution for the Dynamic scenario at the ST site, showing a low MAE of 0.02 m^3/m^3, a B near 1.1, and a CC greater than ~0.7 across all summers. Model performance varies depending on the metric and variable inspected, but is generally consistent across calibration and testing periods, suggesting the model is transferable across the different summer periods. In addition, the model performance in terms of soil moisture is robust with respect to the time scale of evaluation, as shown by the daily averaged statistics in Table 4. Overall, the model captures the major features of the soil moisture data at the ST site, including how certain summer periods have sustained levels of high soil water content (2006–2008), while others experience long interstorm periods with low soil moisture levels (2004, 2009).

The seasonal progression of soil wetting induces a vegetation green-up that increases *ET* in the subtropical scrubland, as depicted across all summers in Figure 6. Only daytime periods are included in the comparison.

Table 4. Model Performance for Periods With Simultaneous Observations and Simulations of Latent Heat Flux, Sensible Heat Flux and Surface Soil Moisture at the ST and MW Sites for the Dynamic Scenario for Both 30 Min and Daily Intervals[a]

	Latent Heat Flux			Sensible Heat Flux			Surface Soil Moisture		
Year	B	MAE (W/m^2) or ($MJ/m^2/d$)	CC	B	MAE (W/m^2) or ($MJ/m^2/d$)	CC	B	MAE (m^3/m^3)	CC
Sinaloan Thornscrub, ST (30 Min Statistics)									
2004	0.53	31.46	0.71	0.72	58.40	0.69	0.90	0.02	0.75
2006	*0.60*	*45.35*	*0.78*	*0.84*	*37.85*	*0.66*	*1.06*	*0.02*	*0.79*
2007	0.87	28.52	0.68	0.46	47.33	0.61	1.05	0.02	0.65
2008	0.51	71.28	0.58	0.13	50.19	0.45	1.08	0.02	0.86
2009	0.58	30.32	0.66	0.48	71.10	0.63	1.14	0.02	0.66
Sinaloan Thornscrub, ST (Daily Statistics)									
2004	0.48	76.63	0.85	0.77	90.73	0.67	0.90	0.02	0.78
2006	*0.64*	*105.32*	*0.94*	*0.84*	*73.87*	*0.78*	*1.05*	*0.02*	*0.84*
2007	0.92	53.02	0.84	0.46	138.66	0.72	1.04	0.02	0.76
2008	0.49	257.79	0.16	0.13	188.14	0.23	1.08	0.02	0.88
2009	0.56	37.47	0.91	0.48	206.36	0.72	1.12	0.02	0.79
Madrean Woodland, MW (30 Min Statistics)									
2008	*0.75*	*62.38*	*0.67*	*0.17*	*62.26*	*0.49*	*0.78*	*0.04*	*0.90*
2009	0.91	39.86	0.57	0.91	74.04	0.59	1.00	0.02	0.74
Madrean Woodland, MW (Daily Statistics)									
2008	*0.75*	*135.33*	*0.46*	*0.18*	*170.60*	*0.31*	*0.77*	*0.05*	*0.93*
2009	1.03	64.00	0.73	0.91	107.84	0.48	0.99	0.02	0.76

[a]Italicized years represent the model calibration periods. The statistical metrics used to measure model performance were bias (B), Mean Absolute Error (MAE), and correlation coefficient (CC). The units of MAE depend on 30 min (W/m^2) or daily ($MJ/m^2/d$) statistics for the latent and sensible heat fluxes.

Latent heat flux (λET, where λ is the latent heat of vaporization) is low prior to the NAM onset (June) in both the observations and model simulations (see 2008 and 2009). As *SM* and NDVI increase, the Dynamic scenario captures well the gradual rise in *ET* and its temporal variations in response to individual storms and dry periods. Reductions in *ET* during late summer are also captured well in response to lower water availability and radiation, as well as the start of vegetation senescence. Table 4 shows the model performance metrics with respect to latent and sensible heat flux (W/m^2) at the ST site at both 30 min and daily scales. For the 30 min statistics, we obtained an average MAE of 41 W/m^2, average B of 0.62, and average CC of 0.68 for λE and an average MAE of 53 W/m^2, average B of 0.53, and average CC of 0.61 for *H* across all summers, consistent with daily total fluxes. Focusing on λE, the Bias indicates that under certain conditions in mid-summer the model underestimates *ET* with respect to observations, as seen in 2008, likely due to an inability of the model to account for transpiration emanating from plant water uptake from deep (>1 m) soil layers occurring when the modeled (1 m) root zone has dried. Despite this, the major features of the seasonal evolution of *ET* and its interannual variation are nevertheless captured with reasonable accuracy to warrant a closer analysis of the underlying soil and vegetation contributions to the total *ET*.

Figure 7 presents the comparison of *ET* and *SM* observations and model simulations at the MW site for 2008 and 2009 using the Dynamic scenario. Only daytime periods are included in the comparison. The wetter summer in 2008 (551 mm) leads to a higher NDVI than in the drier 2009 summer (321 mm), with vegetation greenness slowly increasing during the NAM onset and peaking in mid-August in both periods. Differences in time-varying vegetation parameters in the Dynamic scenario (under the same soil properties of Table 2) are able to capture well the interannual variations in *ET* and *SM*, with wetter soils and higher evapotranspiration losses in 2008 than in 2009. Table 4 shows that the model performance at the Madrean woodland is comparable to the ST site in terms of latent and sensible heat fluxes and surface soil moisture, with a better match during the drier 2009 period, at both 30 min and daily scales. This suggests that model performance may improve in terms of certain variables above the calibration results depending on the meteorological forcing and its subsequent vegetation response. For this ecosystem, the seasonal evolution of *ET* and *SM* are also captured well, as are the hydrologic responses to individual storms and subsequent dry-down periods. It is interesting to note that the MW site experiences higher soil moisture values with lower recession rates as compared to the ST ecosystem. The more frequent, smaller rainfall events at the higher elevation MW site [*Gebremichael et al*., 2007] also permit sustained *ET* throughout the summer season. Although the model captured well the observations overall, it is important to note an underestimation in *ET* in August and September

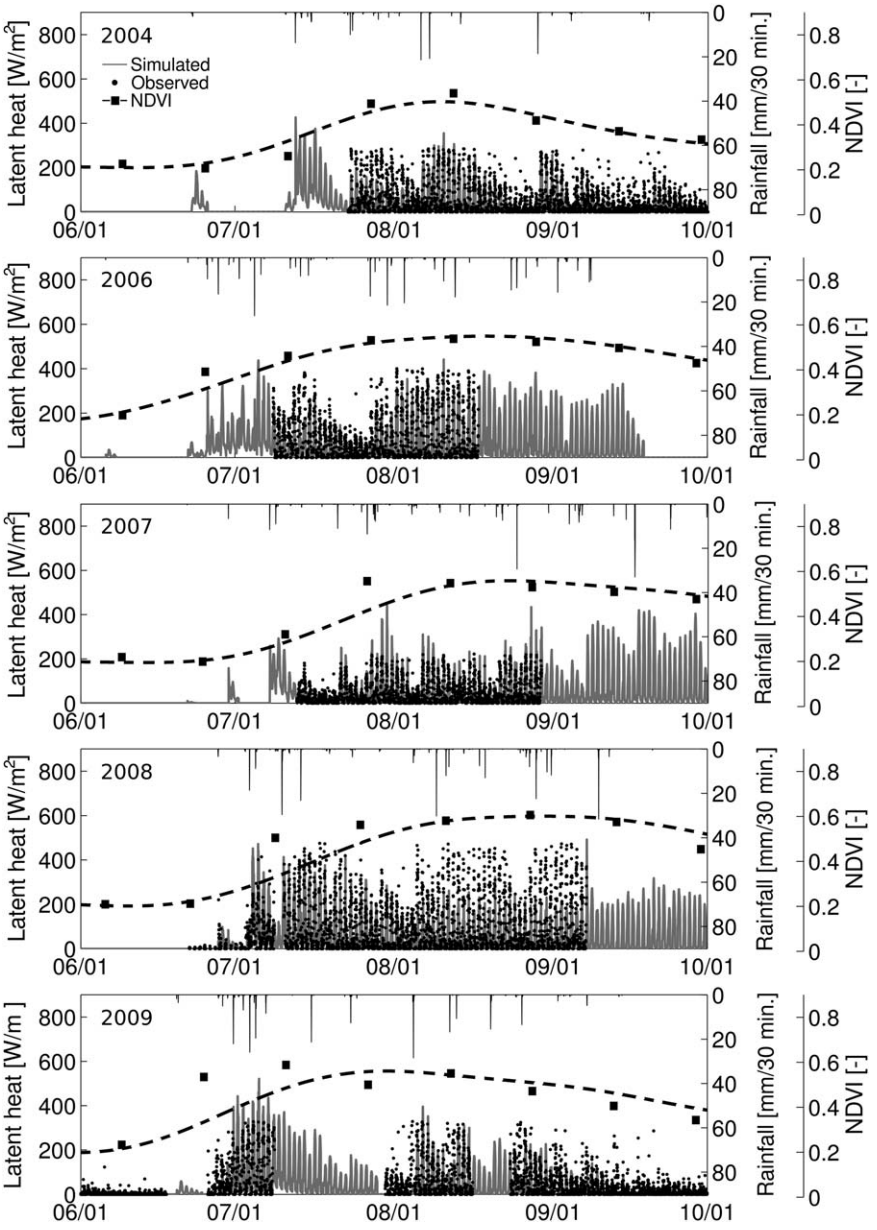

Figure 6. Comparison of observed and simulated latent heat flux at the ST site for 2004 and 2006–2009 under the Dynamic scenario. Gaps in the observations are depicted by missing data. For reference, NDVI shows the vegetation greenness variations at the site with the squares indicating the composite data with the smoothed series as dashed lines.

2008, which are likely related to the high precipitation that year leading to plant water uptake from deep (>1 m) soil layers. In addition, high rainfall conditions and the presence of fog or dew during this period may have interfered with the EC measurements causing unusually large and sustained *ET* observations that were not removed during standard data processing using the quality control method of *Mauder and Foken* [2004]. Among other identified sources of EC measurement error [e.g., *Kochendorfer et al.*, 2012; Frank et al., 2013), the effects of standing water from fog, dew or precipitation on the LI7500 sensor are well known and occur by obstructing passage of the infrared beam [e.g., *Massman and Lee*, 2002].

3.3. Comparisons of *ET-SM* Relation for Vegetation Scenarios

The two static scenarios (Leaf off and Leaf on) allow analyzing the effects of seasonal and interannual variations of vegetation on the hydrologic conditions at the ST and MW sites. For simplicity, these scenarios are described through a comparison of the relation between daily total *ET* and daily averaged *SM* for the top 10

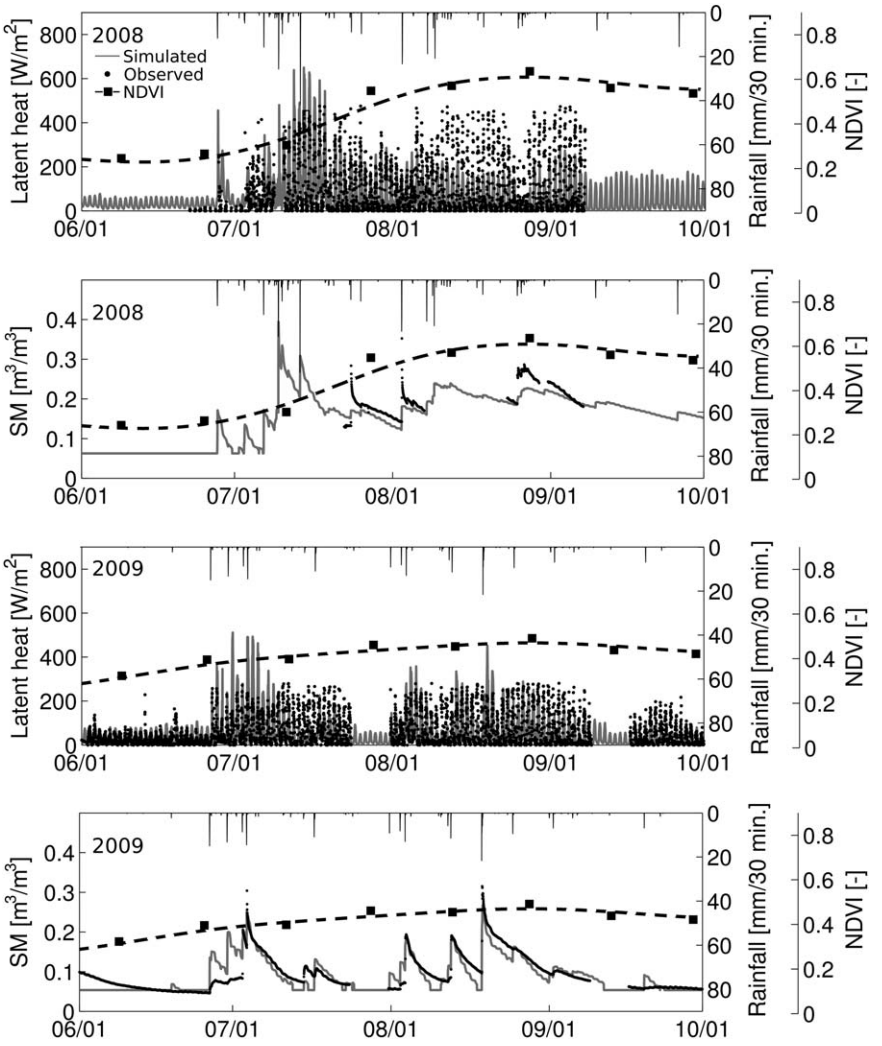

Figure 7. Comparison of observed and simulated latent heat flux and surface soil moisture (*SM*, top 10 cm) at the MW site for 2008–2009. Missing data are due to observational gaps. For reference, NDVI shows the vegetation greenness variations at the site with the squares indicating the composite data and the smoothed series as dashed lines.

cm. Figure 8 presents the *ET-SM* relation for each summer period from the three scenarios as well as the available daily data (not used in the relations). For clarity, the simulations for all summer days are presented as piecewise linear regressions, such that the lines are a visualization tool to compare the scenarios. The regression parameters were identified through a semiautomatic procedure aimed at minimizing the root mean square error (RMSE) between the pair of points (*SM*, *ET*) of the model simulations and the regression lines. Note that the *ET-SM* relations are determined based on all simulated days, while the observations are limited to only days (*n*) with available data. The regressions allow depicting the stressed *ET* (region with positive slope) and the maximum *ET* (region with constant values) corresponding to low and high *SM*. From the observations, it is clear that interannual variations exist in the *ET* and *SM* ranges at both sites, with wetter summers (2006–2008) exhibiting higher values. Due to its adjustment of vegetation parameters each summer, the Dynamic scenario shows interannual differences in the *ET-SM* relation that visually match the observations better than the Leaf off and Leaf on scenarios. This is corroborated by the lower RMSE in daily *ET* between observations and the piecewise linear regressions for the Dynamic scenario. When averaged over all summers and both sites, the Dynamic case has an RMSE of 1.73 mm/d, as compared to 1.93 and 2.93 mm/d for the Leaf off and Leaf on scenarios. The *ET-SM* relation for the Dynamic scenario generally has better performance relative to observations for the calibration periods (2006 at ST and 2008 at MW), with a lower skill in the testing periods.

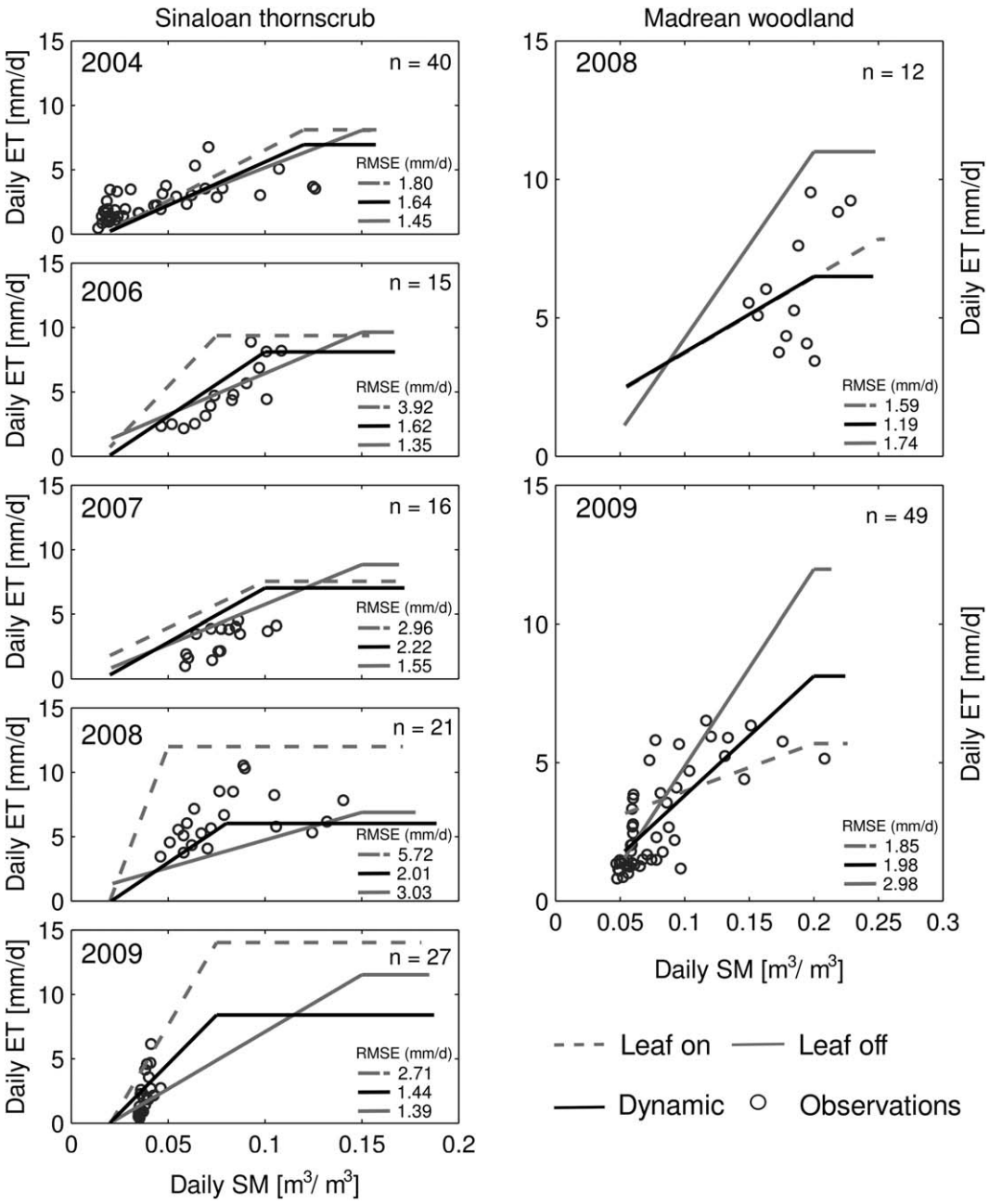

Figure 8. Interannual variability of the relation between daily evapotranspiration and surface soil moisture (*SM*, top 10 cm) for three vegetation scenarios at the ST and MW sites. Daily observations (*n* is the number of available days) are included for comparison (circles) along with the root mean square error (RMSE) in evapotranspiration (mm/d) for the piecewise linear regression in each scenario.

The Leaf on and Leaf off cases present an interesting comparison to the Dynamic scenario in each ecosystem. For the ST site, the Leaf on scenario has the highest *ET* for most *SM* values across all summer periods, indicating the full canopy development in the subtropical scrubland maximizes *ET* losses to the atmosphere and thus lowers *SM*. This suggests that plant transpiration is a more efficient means to extract soil moisture since it acts over a deeper (1 m) profile and has a lower stress factor, β_T (Table 3). In contrast, the Leaf off scenario has the lowest *ET* and highest *SM*, indicating that bare soil conditions at the ST site have lower losses, primarily due to a higher soil evaporation stress factor, β_E (Table 3). Interestingly, the Dynamic scenario has a behavior that suggests that time-varying parameters result in an *ET* bounded by the two other cases, in particular for intermediate soil moisture values (i.e., 0.05–0.125 m^3/m^3).

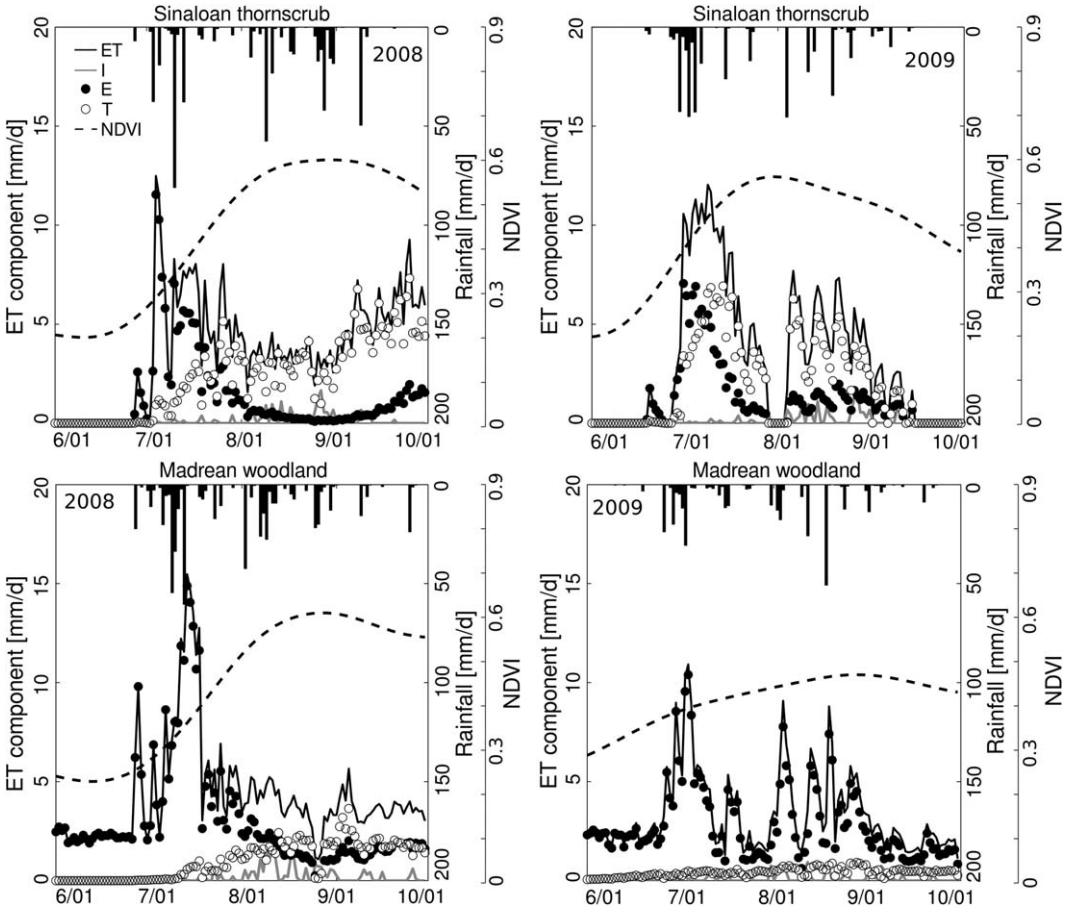

Figure 9. Simulated evapotranspiration partitioning under the Dynamic scenario at the ST and MW sites for 2008 and 2009. For reference, NDVI shows the observed vegetation greenness variations at the sites.

In the oak savanna, comparisons between vegetation scenarios are limited to two summers. The Leaf on and Leaf off scenarios were selected from observations over a period of five summers and as a result represent conditions not necessarily experienced in 2008 and 2009. In contrast to the ST site, the minimum greenness in the Leaf off scenario leads to high *ET* and low *SM*, while the maximum greenness in the Leaf on scenario leads to a lower *ET* and higher *SM*. Here the Dynamic scenario also exhibits an intermediate *ET-SM* relation as compared to the bounds presented by the other cases and matches the field data better when averaged over the two seasons, as shown by the RMSE. Differences between MW and ST in the relative performance of the Leaf off and Leaf on scenarios can be attributed to: (1) higher incoming solar radiation that favors greater *ET* at MW and (2) lower vegetation fraction in the oak savanna. Interestingly, the ability of the Dynamic scenario to adjust the *ET-SM* relation to match the available data indicates that vegetation greening plays a crucial role in modulating losses to the atmosphere in the oak savanna ecosystem. It also reveals that lower vegetation fractions at MW leads to a different behavior as compared to the ST site, with respect to the partitioning of *ET* between vegetation canopies and surrounding bare soil, as will be explored in the following.

3.4. Temporal Variations of *ET* Partitioning

The simulated partitioning of evapotranspiration (Appendix C) permits an evaluation of the effect of vegetation greening on soil and vegetation-mediated processes. Figure 9 presents the simulated *ET* partitioning for two contrasting summers, the wetter 2008 and drier 2009 periods, at the ST and MW sites under the Dynamic scenario. Both summers received rainfall events in late June and early July, but 2008 had more sustained precipitation in late August and September that allowed NDVI to remain higher. Prior to green-up, *ET* is dominated by soil evaporation (*E*) at both sites, as bare soil fractions

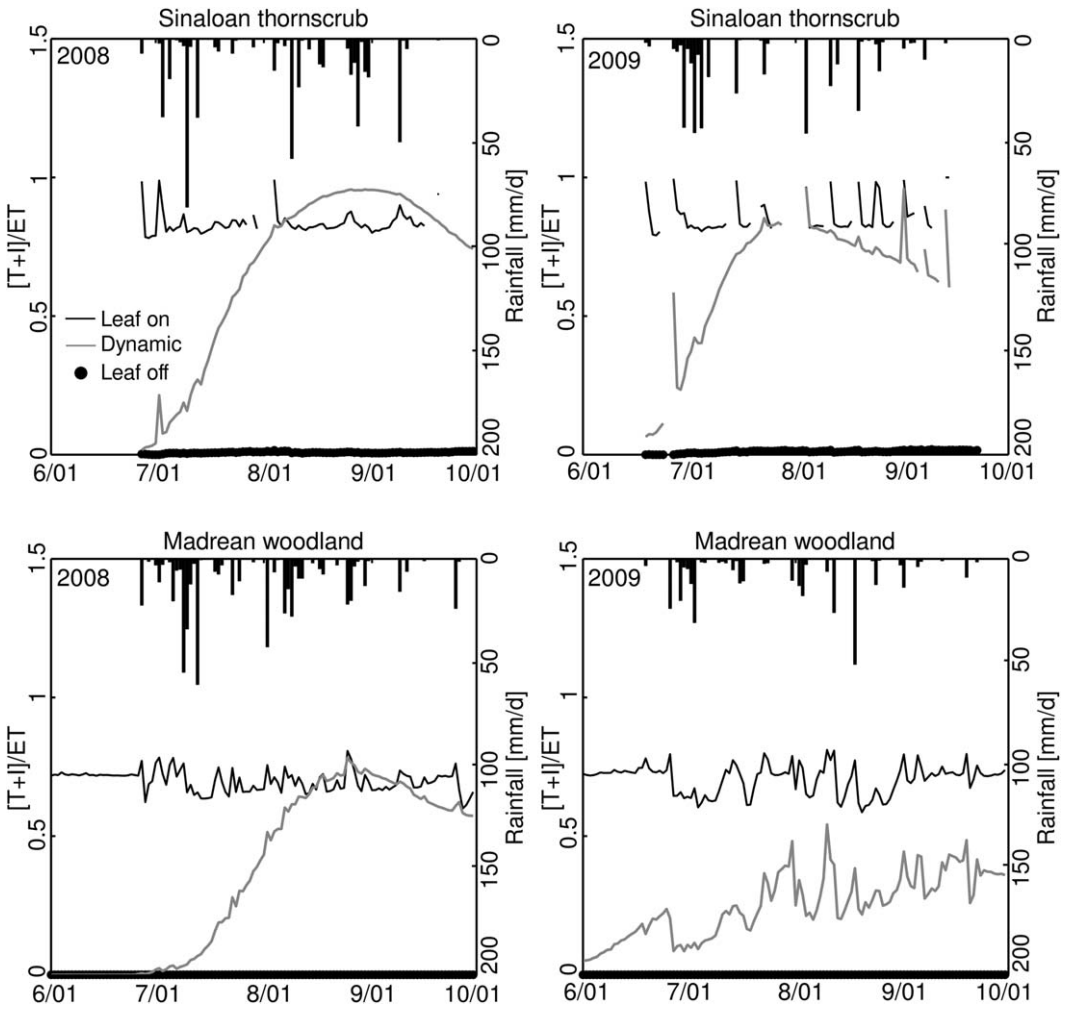

Figure 10. Vegetation-mediated fraction, $(T + I)/ET$, under three vegetation scenarios at the ST and MW sites for 2008 and 2009.

$(1 - v_f)$ are greater than 50%. In the subtropical scrubland, a switch to transpiration (T) dominance was simulated after early to mid-July, reaching values of 5–7 mm/d in each summer, with an earlier green-up and a quicker transition to transpiration in 2009. In contrast, the oak savanna exhibited this switch only in the wetter 2008 period. The late greening and low NDVI at MW in 2009 resulted in higher soil evaporation rates throughout the season. During the late summer, precipitation determines whether ET is sustained (as in 2008) or rapidly decays (as in 2009), while the partitioning begins to favor E as NDVI decreases in response to lower radiation. Overall, transpiration rates at MW were consistently lower than at ST and contributed a lower fraction of the total ET. Since total ET averaged over all summers was higher at MW (465 mm) than at ST (422 mm), E plays a dominant role in the oak savanna due to a sparser plant cover. As expected, the evaporation of intercepted water (I) had a small contribution to ET with maximum values of 2 mm/d during periods of higher v_f.

The impact of the vegetation greening on the ET partitioning is presented in Figure 10 by comparing the vegetation scenarios in terms of the vegetation-mediated fractions or $(T + I)/ET$. Vegetation-mediated processes are typically dominated by transpiration and E/ET can be obtained as $1 - (T + I)/ET$. The comparison in Figure 10 includes both the ST and MW sites for the wetter 2008 and drier 2009 summer periods. Note that the Leaf off scenario was entirely dominated by E/ET such that $(T + I)/ET$ was near zero for all cases. Similarly, the Leaf on scenario exhibited $(T + I)/ET$ primarily between 0.8 and 1 (ST) and 0.5 and 0.7 (MW), indicating a significantly lower contribution of E/ET at ST and a larger E/ET at MW. As such, the Leaf off and Leaf on scenarios are considered as hypothetical bounds on the actual ET partitioning

for each ecosystem under variable (day-to-day) meteorological forcing. The Dynamic scenario, on the other hand, represents well the seasonal evolution and interannual variations in *ET* partitioning. $(T + I)/ET$ exhibits a gradual increase in response to vegetation green-up and a peak amount and timing that varies according to the seasonal distribution of rainfall events. During peak greenness, $(T + I)/ET$ can range from 0.5 to 1, with higher contributions at ST and for wetter periods. Interestingly, the day-to-day variations in $(T + I)/ET$ seem to be higher for the drier 2009 period at both sites, indicating that lower vegetation greenness leads to higher susceptibility to decreases in vegetation-mediated processes during interstorm periods. The drier summer also has a lower seasonal recession of $(T + I)/ET$ in each ecosystem. This indicates that *ET* partitioning is highly variable within and across summer seasons in response to vegetation differences.

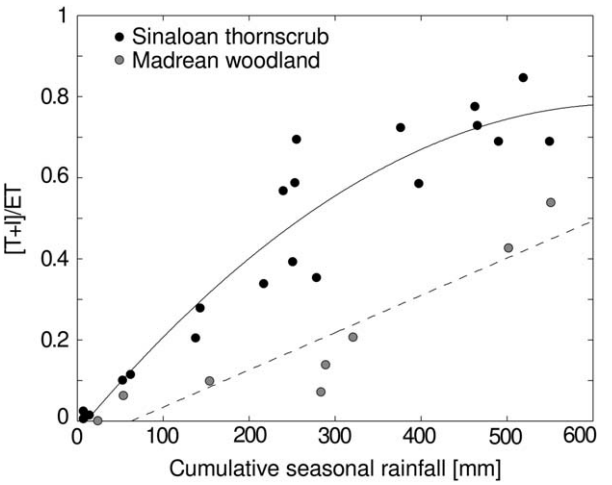

Figure 11. Relation of vegetation-mediated fraction, $(T + I)/ET$, with cumulative seasonal rainfall, defined as the current and prior month totals. The black solid line is a regression for ST, while the gray dashed line is a regression for MW.

3.5. Comparison of *ET* Partitioning in Two Ecosystems

The analysis over multiple summers in the two ecosystems allows determining the impact of seasonal rainfall amounts on the partitioning of evapotranspiration. Establishing this relation would allow for a simple approach for estimating the vegetation effects on *ET* based on available rainfall data for the two different ecosystems. Figure 11 shows the relation between the monthly vegetation-mediated losses to the atmosphere, $(T + I)/ET$, and the cumulative rainfall over the current and previous months (P_{accm}) and the best-fit regressions obtained over a range of possible models. The ST site shows an asymptotic relation between $(T + I)/ET$ and P_{accm} over the five summer periods ($n = 20$ based on 4 months in five summers; $(T + I)/ET = -2.0 \times 10^{-6} P_{accm}{}^2 + 2.5 \times 10^{-3} P_{accm} - 2.4 \times 10^{-2}$, $R^2 = 0.95$). In contrast, the MW site exhibits a linear increase in $(T + I)/ET$ with the cumulative rainfall ($n = 8$ for 4 months in two summers; $(T + I)/ET = 9.2 \times 10^{-4} P_{accm} - 5.7 \times 10^{-2}$, $R^2 = 0.92$). In both cases, higher accumulated precipitation leads to a greater amount of vegetation-mediated processes due to the production of biomass supporting transpiration and evaporation of intercepted rainfall. For the subtropical scrubland, however, a threshold of 390 mm in 2 month total rainfall yields a change in the slope of the $(T + I)/ET$ relation with P_{accm}, as compared to the linear increase in the MW site, indicating that additional rainfall does not appreciably increase vegetation-mediated losses. Nevertheless, the ST site sustains higher $(T + I)/ET$ than the MW site at all rainfall amounts, indicating that subtropical scrublands have a greater ability to return soil moisture back to the atmosphere through $(T + I)/ET$. Since plant interception is larger at the MW site, this implies that transpiration at the ST site is more sensitive to low rainfall (higher slope for $P_{accm} < 390$ mm), while being less sensitive at higher accumulations (lower slope for $P_{accm} > 390$ mm), as compared to MW.

The differences in *ET* partitioning in the two ecosystems are further explored in Figure 12 as the time-averaged seasonal evolution of T/T_{max} and E/E_{max}, where normalization is performed with maximum values over all summers. Time-averaged NDVI/NDVI_{max} is also shown to indicate vegetation green-up onset and duration. Note that the seasonal evolution of E/E_{max} and T/T_{max} are inversely related since these losses represent the primary *ET* components (Table 5). The subtropical scrubland and oak savanna are both characterized by high E/E_{max} in the early summer prior to the onset of greening. At the ST site, the earlier and faster increase in NDVI to maximum canopy development ($\text{NDVI}/\text{NDVI}_{\text{max}} = 1$) yielded a quicker transition toward high T/T_{max} that is sustained throughout the summer. In contrast, the delayed green-up at the MW site results in high T/T_{max} only toward the end of the season, indicating that soil-mediated processes are significant in the oak savanna during a larger fraction of the summer as

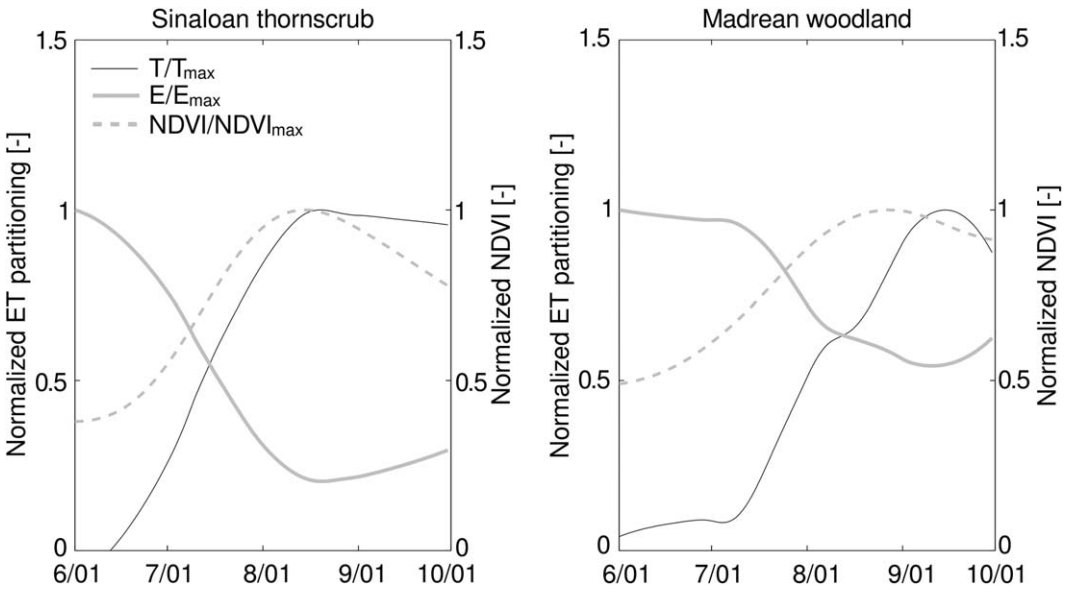

Figure 12. Seasonal evolution of normalized evapotranspiration components (T/T_{max} and E/E_{max}) and NDVI/NDVI$_{max}$ at the ST and MW sites averaged over available seasons.

compared to the ST site (Table 5). As expected, the peak transpiration losses, $T/T_{max} = 1$, occur after the peak NDVI in both ecosystems as it takes times for vegetation greening to impact water and energy fluxes at each site. Interestingly, the delay between peak NDVI/NDVI$_{max}$ and peak T/T_{max} is on the order of 5 days in the subtropical scrubland and nearly three weeks (20 days) in the oak savanna. This indicates that the MW site has a slower transpiration response to rainfall during the North American monsoon leading to a higher proportion of soil-mediated losses, as summarized in Table 5. Toward the end of the summer, E/E_{max} begins to increase in both ecosystems in response to the beginning of vegetation senescence, which lasts for different periods of time in each ecosystem [*Méndez-Barroso et al*., 2009; *Forzieri et al*., 2011].

4. Discussion and Conclusions

Seasonal vegetation greening affects the partitioning of water and energy fluxes in arid and semiarid ecosystems under the influence of the North American monsoon [e.g., *Reynolds et al*., 2000; *Yépez et al*., 2003, 2007; *Scott et al*., 2006; *Watts et al*., 2007; *Vivoni*, 2012]. As a result, modeling applications that assume constant parameters or represent each summer with a fixed seasonal cycle can miss important vegetation impacts. In this study, we compared simulations that capture seasonally varying parameters inferred from remotely sensed data to static scenarios representing no canopy and full canopy conditions for two ecosystems that are representative of intermediate and high elevation landscapes along mountain fronts in the North American monsoon region. We found good agreement between field observations of

Table 5. Evolution of Monthly *ET* Partitioning into Soil Evaporation (*E*), Plant Transpiration (*T*), and Evaporation of Intercepted Rainfall (*I*) for the ST and MW Sites[a]

	Sinaloan Thornscrub			Madrean Woodland		
Month	*E/ET* (%)	*T/ET* (%)	*I/ET* (%)	*E/ET* (%)	*T/ET* (%)	*I/ET* (%)
Jun	90.3	7.8	1.9	96.4	3.3	0.3
Jul	58.3	38.9	2.8	89.8	8.2	1.9
Aug	23.7	70.8	5.6	64.3	26.8	8.9
Sep	26.4	70.8	3.7	53.8	41.9	4.3
Total	39.0	57.4	3.7	77.4	18.6	4.0

[a]Seasonal totals are shown as "Total." Values represent averages over all summer periods.

evapotranspiration and soil moisture and simulations from Dynamic scenarios, indicating that the hydrologic model can represent interannual differences in the water and energy fluxes in the two ecosystems. In contrast, the Leaf off and Leaf on scenarios had a limited ability to track the seasonal evolution and interannual differences in *ET* and *SM* responding to precipitation-induced vegetation variations. While this result is robust over the five summer period in the subtropical scrubland (ST site), additional data in the oak savanna (MW site) would be valuable for quantifying interannual ecosystem adjustments.

Precipitation events during the North American monsoon wet surface soils and induce a vegetation response that varies substantially across the two ecosystems. Early in the monsoon season, however, both ecosystems have dormant plants and soil evaporation is the dominant *ET* component. The switch toward transpiration dominance occurs differentially in each ecosystem such that it takes 2–3 weeks for the full transition to take place in the subtropical scrubland and 6–8 weeks in the oak savanna. These model-based estimates are consistent with field data in arid and semiarid ecosystems that respond to the North American monsoon [e.g., *Mielnick et al*., 2005; *Scott et al*., 2006; *Yépez et al*., 2007; *Cavanaugh et al*., 2011]. Furthermore, the model identified, for the first time, that the peak transpiration losses are delayed by 5 days and 20 days, on average, from the peak NDVI at the ST and MW sites, respectively. A longer lag time between peak NDVI and transpiration at the MW site as compared to the ST site is likely due to the slower production of more costly leaves and ensuing activation of the photosynthetic process. This also suggests that rapid and robust vegetation greening in subtropical scrublands is linked directly to the dominance of vegetation-mediated losses, where T/ET was found to be $56 \pm 9\%$ over the five summer periods, well within the range of values at shrubland sites with a high vegetation cover [e.g., *Scott et al*., 2006]. Recent efforts by *Tarín et al.* [2014] using an isotopic partitioning method found $T/ET = 59 \pm 6\%$ at ST for four specific days. Model comparisons for these days revealed a standard error of estimates (SEE) of 0.16, with the match varying from a 16% to a 40% difference for individual days. This suggests that the model is capturing *ET* partitioning well under the limited conditions of the available data for the study periods. In contrast, delayed and attenuated vegetation greening in the oak savanna is responsible for soil-mediated losses having a dominant role throughout the season, with T/ET of only $18 \pm 8\%$. The important role of soil evaporation in oak savannas has been recognized previously by *Baldocchi and Xu* [2007] and *Pereira et al*. [2009], but not placed in the context of summer vegetation greening. Overall, the seasonal evolution of *ET* components indicates that transpiration is in-phase with vegetation greenness at the ST site, but out-of-phase (or delayed) at the MW site, a significant new insight provided through the model. This is consistent with a stronger link between cumulative precipitation and vegetation-mediated losses, $(T + I)/ET$, in subtropical scrublands as compared to oak savannas.

Based on long-term analyses of vegetation greening, *Forzieri et al.* [2011] found that deciduous subtropical ecosystems in the NAM region have high seasonality with a short period of intense greening occurring rapidly after precipitation onset. Mountain woodlands including oak savannas, on the other hand, were found to have more a prolonged period of moderate greenness that was delayed with respect to the precipitation onset but continued well into the fall season. Results described in this study identify the implications of the two ecosystem types on the water and energy fluxes, specifically on evapotranspiration and its partitioning, which have not been previously known. Intermediate-elevation subtropical scrublands have a high sensitivity to precipitation, primarily during the early development of the NAM, that allow them to quickly transition from soil to vegetation-mediated losses to the atmosphere. These intensive water users rapidly deplete available soil moisture through transpiration, subsequently leading to decreases in vegetation greenness and transpiration near the end of the summer. In contrast, high-elevation oak savannas, with a lower sensitivity of canopy development to precipitation, have a slower transition from evaporation to transpiration-dominated periods. As a result, these extensive water users slowly deplete soil moisture during the NAM, preserving it for subsequent use to maintain greenness and transpiration during the fall. As discussed by *Rodríguez-Iturbe et al*. [2001], variations in plant water use between intensive and extensive strategies may allow different ecosystems to occupy specific niches along the mountain front.

The noted variations in seasonal and interannual dynamics of *ET* and its components in the two ecosystems have a number of implications on the ecological and hydrologic properties of semiarid mountain fronts in the NAM region. First, the switch from soil to vegetation-mediated losses affects soil moisture storage since evaporation is primarily sourced from shallower layers. The delayed transition at higher elevations implies that deeper soil water is preserved for longer periods, potentially leading to mountain recharge [*Wilson and Guan*, 2004]. Second, the rapid transition toward transpiration in subtropical scrublands implies these sites

are more likely to be responsible for the precipitation-soil moisture-vegetation feedback mechanism [*Dominguez et al*., 2008; *Méndez-Barroso and Vivoni*, 2010]. Thus, the local precipitation recycling that sustains vegetation greening during the NAM may be sourced primarily from intermediate elevations along mountain fronts rather than higher elevations. Finally, spatially variable consumption of precipitation in the different ecosystems through *ET* may have implications on runoff production [*Robles-Morua et al*., 2012]. However, the underlying processes that could distinguish runoff in subtropical scrublands and oak savannas have yet to be elucidated. Further, the model findings on the interannual variations of *ET* partitioning in the two ecosystems need to be corroborated by additional field studies, in particular at high elevation oak savannas. As demonstrated in this work, the comparative analysis of evapotranspiration and its partitioning in different ecosystems through the use of field observations, remote sensing estimates, and hydrological modeling is a fruitful avenue of future work.

Appendix A

Three evaporation components are estimated in tRIBS: (1) bare soil evaporation (E), (2) evaporation of canopy interception (I), and (3) plant transpiration (T). Total evapotranspiration ($ET = E + I + T$) is estimated in a stepwise fashion using the Penman-Monteith approach:

$$\lambda ET = \frac{\frac{\Delta}{\gamma}(R_n - G) + \frac{\rho_m \lambda}{r_a}\delta q_a}{1 + \frac{\Delta}{\gamma} + \frac{r_s}{r_a}}, \tag{A1}$$

where Δ is the slope of the Clausius-Clayperon relation, γ is the psychometric constant, λ is the latent heat of vaporization, R_n is the net radiation, G is the ground heat flux, ρ_m is the moist air density, δq_a is the specific humidity deficit, and r_a and r_s are the aerodynamic and canopy stomatal resistances. r_a is estimated using wind speed observations and vegetation height (h) estimates under the assumption of a logarithmic velocity profile [*Shuttleworth*, 1992]. In this study, the time-varying r_s is obtained from remotely sensed measurements of LAI and fPAR (see Appendix C). Net radiation is impacted by the albedo (a) and optical transmission coefficient (k_t) that characterize the plant canopy or soil surface (Table 3).

Interception occurs as a fraction of rainfall, $(1 - p)R$, where p is the free throughfall coefficient and R is rainfall. Evaporation of intercepted water on the canopy is fulfilled first in the stepwise calculations as [*Eltahir and Bras*, 1993]:

$$I = \begin{cases} v_f E_p & for \quad C > S \\ \frac{C}{S} v_f E_p & for \quad C \leq S \end{cases}, \tag{A2}$$

where C is the canopy storage volume, S is the maximum canopy storage (Table 3), and E_p is the potential evaporation rate that excludes the effect of canopy stomatal resistance obtained as:

$$E_p = ET\left[\frac{\Delta + \gamma(1 + r_s/r_a)}{\Delta + \gamma}\right]. \tag{A3}$$

The *Rutter et al*. [1971] approach to tracking the canopy water storage is utilized in the model.

Bare soil evaporation is then obtained for the bare soil fraction, independently of the plant transpiration, from the potential evaporation rate as [*Deardorff*, 1978]:

$$E = (1 - v_f)\beta_S E_p, \tag{A4}$$

where v_f is the vegetation fraction of a model element occupied by a plant functional type (i.e., tree or shrub) and represents the green vegetation cover that can be linked to NDVI (Appendix C), while $1 - v_f$ represents the bare soil area, and β_S is a function of soil moisture as:

$$\beta_S = \min\left(1, \frac{\theta_{sur} - \theta_r}{\beta_E \theta_s - \theta_r}\right), \tag{A5}$$

where θ_{sur} is the surface soil moisture (top 10 cm), θ_s is the soil moisture at saturation, θ_r is the residual soil moisture, and β_E is the soil evaporation stress factor (Tables 2 and 3). The form of A5 is commonly used in hydrologic models [see *Feddes et al*., 1978; *Mahfouf et al*., 1996].

Plant transpiration (T) is calculated after accounting for the consumption of intercepted water by evaporation as:

$$T = \beta_R v_f (E_p - I)\left[\frac{\Delta + \gamma}{\Delta + \gamma(1 + r_s/r_a)}\right], \tag{A6}$$

where β_R accounts for soil moisture stress that limits the plant water uptake as:

$$\beta_R = \min\left(1, \frac{\theta_{root} - \theta_r}{\beta_T \theta_s - \theta_r}\right), \tag{A7}$$

where θ_{root} is the root zone moisture (top 1 m) and β_T is the plant transpiration stress factor. Thus, ET is composed of three components ($ET = E + I + T$) that depend on vegetation (v_f, r_s, p, S, β_E, and β_T) and soil (θ_s and θ_r) properties, including soil moisture, as well as meteorological forcing, through a weighting based on the areal proportions of bare soil and vegetation. For additional information, the reader is referred to *Wigmosta et al*. [1994] and *Ivanov et al*. [2004].

Appendix B

Model performance is assessed using three metrics to compare observations (O) and simulations (S) of latent heat flux and soil moisture over the number of time steps (N) with available data. The Mean Absolute Error (MAE) describes the absolute differences between observations and simulations without emphasizing the value of outliers as:

$$MAE = \frac{1}{N}\sum_{i=1}^{N} |O_i - S_i|. \tag{B1}$$

The correlation coefficient (CC), which measures the linear relation between S and O, is:

$$CC = \frac{\sum_{i=1}^{N}(O_i - \bar{O})(S_i - \bar{S})}{\left[\sum_{i=1}^{N}(O_i - \bar{O})^2\right]^{0.5}\left[\sum_{i=1}^{N}(S_i - \bar{S})^2\right]^{0.5}}, \tag{B2}$$

where the overbar denotes a temporal mean value. CC varies from -1 (negative correlation) to 1 (positive correlation), with CC = 0 indicating no correlation. The dimensionless bias (B) is obtained as the ratio of temporal mean of the simulated and observed variables, as:

$$B = \frac{\bar{S}}{\bar{O}}. \tag{B3}$$

Appendix C

A set of empirical equations are used to link remote sensing data to vegetation parameters in tRIBS (Table 3). In each case, coefficient values were locally calibrated by comparing the retrieved parameters to the range of values from available literature in similar ecosystems. Maximum canopy storage (S) controls rainfall interception as a function of time-varying LAI from MODIS. For both sites, we used the relation, $S = 0.5\mathrm{LAI}$,

from *Pitman* [1989] and *Carlyle-Moses and Price* [2007], with the coefficient verified with the data sets of *Pitman* [1989] for shrubs and *Andre et al.* [2008] for oaks. The free throughfall coefficient (p) accounts for the fraction of rainfall not captured by plants. We relate p to time-varying LAI, following *Pitman* [1989], as:

$$p = \exp(-1.5LAI) \tag{C1}$$

The optical transmission coefficient (k_t) is obtained from the Beer-Lambert law as:

$$k_t = \exp(-kLAI) \tag{C2}$$

where $k = 0.61$ for ST [*Maass et al.*, 1995] and $k = 0.31$ for MW [*Sugiyama et al.*, 1985], based on differences in leaf architecture at the two sites. The minimum canopy stomatal resistance (r_s) was obtained using an energy-limited relation developed by *Schulze et al.* [1995] and upscaled from an individual leaf to the canopy following *Irmak et al.* [2008]:

$$r_s = \frac{\left[\frac{Q_{50}+Q}{g_{\max} Q}\right]}{LAI}, \tag{C3}$$

where g_{max} is the maximum seasonal stomatal conductance specified as 0.03 m/s for drought deciduous trees [*Schulze et al.*, 1995] and assumed here to be constant in time and for different vegetation types. A diurnal cycle is prescribed for stomatal resistance such that the minimum value (r_s) occurs at noon. This relation does not account for atmospheric conditions that are treated separately in the evapotranspiration estimate (A1). Q_{50} is the value of the absorbed photosynthetically active radiation (Q) obtained when g_{max} is half of its value. Q is obtained as:

$$Q = 0.45 I_S fPAR, \tag{C4}$$

where I_s is the incoming shortwave radiation, fPAR is the fraction of photosynthetically active radiation from MODIS and the coefficient 0.45 represents the fraction of I_s that is used by plants directly for photosynthesis [*Meek et al.*, 1984]. Minimum stomatal resistance values (r_s) for both sites were calibrated using the global estimates of *Dorman and Sellers* [1989]. Vegetation fraction (v_f) was estimated following *Carlson and Ripley* [1997] as:

$$v_f = \left[\frac{NDVI - NDVI_{\min}}{NDVI_{\max} - NDVI_{\min}}\right]^2, \tag{C5}$$

where $NDVI_{min}$ and $NDVI_{max}$ are the minimum and maximum values of the time-varying NDVI obtained over the MODIS record (2004–2009) at each site. $NDVI_{min}$ and $NDVI_{max}$ represent the background signal from the soil during the driest period of the record and peak greenness during the wettest period of the record [*Méndez-Barroso et al.*, 2009]. In the model, the vegetated fraction carries out transpiration, while the 1-v_f fraction is considered to be bare soil and is subject to soil evaporation (Appendix A). Time-varying albedo (a) was obtained directly from MODIS. Other vegetation parameters, such as vegetation height (h), were kept constant in the simulations.

Acknowledgments
We acknowledge funding from the NOAA Climate Program Office (GC07–019), NSF IRES Program (OISE 0553852), and a Consejo Nacional de Ciencias y Tecnología (CONACY) fellowship. We thank students from the United States and Mexico who participated in the field work. Three anonymous reviewers provided excellent comments that helped improve the manuscript.

References

Andre, F., M. Jonard, and Q. Ponette (2008), Precipitation water storage capacity in temperate mixed Oak-Beech canopy, *Hydrol. Processes*, *22*, 4130–4141.

Arora, V. (2002), Modeling vegetation as a dynamic component in soil-vegetation-atmosphere transfer schemes and hydrological models, *Rev. Geophys.*, *40*(2), 1006, doi:10.1029/2001RG000103.

Baldocchi, D. D., and L. Xu (2007), What limits evaporation from Mediterranean oak woodlands: The supply of moisture in the soil, physiological control by plants or the demand by the atmosphere?, *Adv. Water Resour.*, *30*, 2113–2122.

Baldocchi, D. D., B. E. Law, and P. M. Anthoni (2000), On measuring and modeling energy fluxes above the floor of a homogeneous and heterogeneous conifer forest, *Agric. For. Meteorol.*, *102*, 187–206.

Bindlish, R., T. J. Jackson, A. J. Gasiewski, B. Stankov, M. H. Cosh, I. Mladenova, E. R. Vivoni, V. Lakshmi, C. J. Watts, and T. Keefer (2008), Aircraft-based soil moisture retrievals in mixed vegetation and topographic conditions, *Remote Sens. Environ.*, *112*, 375–390.

Brown, D. (1994), *Biotic Communities: Southwestern United States and Northwestern Mexico*, 315 pp., Univ. of Utah Press, Salt Lake City.

Campbell Scientific, Inc. (2012), *Soil Heat Flux Plate Model HFP01, Instruction Manual*, 18 pp., Campbell Scientific (Canada), Edmonton, Alberta, Canada.

Carlson, T. N., and D. A. Ripley (1997), On the relation between NDVI, fractional vegetation cover, and leaf area index, *Remote Sens. Environ.*, *62*, 241–252.

Carlyle-Moses, D. E., and A. G. Price (2007), Modeling canopy interception loss from a Madrean pine-oak stand, Northeastern Mexico, *Hydrol. Processes*, *21*, 2572–2580.
Cavanaugh, M., S. Kurc, and R. L. Scott (2011), Evapotranspiration partitioning in semiarid shrubland ecosystems: A two-site evaluation of soil moisture control on transpiration, *Ecohydrology*, *4*, 671–681.
Cleugh, H. A., R. Leuning, Q. Mu, and S. W. Running (2007), Regional evaporation estimates from flux tower and MODIS satellite data, *Remote Sens. Environ.*, *106*, 285–304.
Deardorff, J. W. (1978), Efficient prediction of ground surface temperature and moisture with inclusion of a layer of vegetation, *J. Geophys. Res.*, *82*, 1889–1903.
Dorman, J. L., and P. J. Sellers (1989), A global climatology of albedo, roughness length and stomatal resistance for atmospheric general circulation models as represented by Simple Biosphere Model (SiB), *J. Appl. Meteorol.*, *28*, 833–855.
Eltahir, E. A. B. (1998), A soil moisture-rainfall feedback mechanism, theory and observations, *Water Resour. Res.*, *34*, 765–776.
Eltahir, E. A. B., and R. L. Bras (1993), A description of rainfall interception over large areas, *J. Clim.*, *6*, 1002–1008.
Feddes, R. A., P. J. Kowalik, and H. Zaradny (1978), *Simulation of Field Water Use and Crop Yield*, 188 pp., John Wiley, New York.
Fensholt, R., I. Sanholt, and M. Schultz (2004), Evaluation of MODIS LAI, fAPAR and the relation between fAPAR and NDVI in a semiarid environment using in situ measurements, *Remote Sens. Environ.*, *91*, 490–507.
Forzieri, G., F. Castelli, and E. R. Vivoni (2011), Vegetation dynamics within the North American monsoon region, *J. Clim.*, *24*(6), 1763–1783.
Frank, J., W. Massman, and B. Ewers (2013), Underestimates of sensible heat flux due to vertical velocity measurement errors in non-orthogonal sonic anemometers, *Agric. For. Meteorol.*, *171–172*, 72–81.
Gebremichael, M., E. R. Vivoni, C. J. Watts, and J. C. Rodríguez (2007), Sub-mesoscale spatiotemporal variability of North American monsoon rainfall over complex terrain, *J. Clim.*, *20*(9), 1751–1773.
Gutzler, D. S. (2004), An index of interannual precipitation variability in the core of the North American monsoon region, *J. Clim.*, *17*, 4473–4480.
Higgins, R. W., and W. Shi (2001), Intercomparison of the principal modes of interanual and intraseasonal variability of the North American monsoon system, *J. Clim.*, *14*, 403–417.
Irmak, S., D. Mutiibwa, A. Irmak, T. J. Arkebauer, A. Weiss, D. L. Martin, and D. E. Eisenhauer (2008), On the scaling up leaf stomatal resistance to canopy resistance using photosynthetic photon flux density, *Agric. For. Meteorol.*, *148*, 1034–1044.
Ivanov, V. Y., E. R. Vivoni, R. L. Bras, and D. Entekhabi (2004), Catchment hydrologic response with a fully distributed triangulated irregular network model, *Water Resour. Res.*, *40*, W11102, doi:10.1029/2004WR003218.
Ivanov, V. Y., R. L. Bras, and E. R. Vivoni (2008), Vegetation-hydrology dynamics in complex terrain of semiarid areas. I: A mechanistic approach to modeling dynamic feedbacks, *Water Resour. Res.*, *44*, W03429, doi:10.1029/2006WR005588.
Kochendorfer, J., T. P. Meyers, J. Frank, W. J. Massman, and M. W. Heuer (2012), How well can we measure the vertical wind speed? Implications for fluxes of energy and mass, *Boundary Layer Meteorol.*, *145*(2), 383–398.
Kustas, W. P., J. H. Prueger, J. L. Hatfield, K. Ramalingam, and L. E. Hipps (2000), Variability in soil heat flux from a mesquite dune site, *Agric. For. Meteorol.*, *103*, 249–264.
Lapham, W. W. (1989), Use of temperature profiles beneath streams to determine rates of vertical groundwater flow and vertical hydraulic conductivity, *USGS Water Supply Pap.*, *2337*, 1–35.
Lawrence, D., P. Thornton, K. Oleson, and G. Bonan (2007), The partition of evapotranspiration into transpiration, soil evaporation, and canopy evaporation in GCM: Impacts on land-atmosphere interactions, *J. Hydrometeorol.*, *8*, 862–880.
Lee, X., J. Finnigan, and K. T. Paw U (2004), Coordinate systems and flux bias error, in *Handbook of Micrometeorology: A Guide for Surface Flux Measurements*, edited by X. Lee, W. J. Massman, and B. E. Law, pp. 33–66, Kluwer Acad., Dordrecht, Netherlands.
Lizárraga-Celaya, C., C. J. Watts, J. C. Rodríguez, J. Garatuza- Payán, R. L. Scott, and J. A. Sáiz-Hernández (2010), Spatio-temporal variations in surface characteristics over the North American monsoon region, *J. Arid Environ.*, *74*, 540–548.
Maass, J. M., J. M. Vose, W. Swankb, and A. Martinez-Yrizar (1995), Seasonal changes of leaf area index (LAI) in a tropical deciduous forest in west Mexico, *For. Ecol. Manage.*, *74*, 171–180.
Mahfouf, J.-F., C. Ciret, A. Ducharne, P. Irannejad, J. Noilhan, Y. Shao, P. Thorton, Y. Xue, and Z.-L. Yang (1996), Analysis of transpiration results from the RICE and PILPS Workshop, *Global Planet. Change*, *13*, 73–88.
Massman, W. J., and X. Lee (2002), Eddy covariance flux corrections and uncertainties in long-term studies of carbon and energy exchanges, *Agric. For. Meteorol.*, *113*, 121–144.
Matsui, T., V. Lakshmi, and E. E. Small (2005), The effects of satellite derived vegetation cover variability on simulated land-atmosphere interactions in the NAMS, *J. Clim.*, *18*, 21–40.
Mauder, M., and T. Foken (2004), *Documentation and Instruction Manual of the Eddy Covariance Software Package TK2*, vol. 26, 44 pp., Univ. Bayreuth, Abt. Mikrometeorologie, Bayreuth, Germany.
Meek, D. W., J. L. Hatfield, T. A. Howell, S. B. Idso, and R. J. Reginato (1984), A generalized relationship between photosynthetically active radiation and solar radiation, *Agron. J.*, *76*, 939–945.
Méndez-Barroso, L. A., E. R. Vivoni, C. J. Watts, and J. C. Rodríguez (2009), Seasonal and interannual relations between precipitation, soil moisture and vegetation dynamics in the North American monsoon region, *J. Hydrol.*, *377*, 59–70.
Méndez-Barroso, L. A., and E. R. Vivoni (2010), Observed shift in land surface conditions during the North American monsoon: Implications for a vegetation-rainfall feedback mechanism, *J. Arid Environ.*, *74*, 549–555.
Mielnick, P., D. A. Dugas, K. Mitchell, and K. Havstad (2005), Long-term measurements of CO_2 flux and evapotranspiration in a Chihuahuan desert grassland, *J. Arid Environ.*, *60*, 423–436.
Mitchell, K. E., et al. (2004), The multi-institution North American Land Data Assimilation System (NLDAS): Utilizing multiple GCIP products and partners in a continental distributed hydrological modeling system, *J. Geophys. Res.*, *109*, D07S90, doi:10.1029/2003JD003823.
Moncrieff, J. B., P. G. Jarvis, and R. Valentini (2000), Canopy fluxes, in *Methods in Ecosystem Science*, edited by O. E. Sala, pp. 161–181, Springer, New York.
Moran, M. S., R. L. Scott, T. O. Keefer, W. E. Emmerich, M. Hernandez, G. S. Nearing, G. B. Paige, M. H. Cosh, and P. E. O'Neill (2009), Partitioning evapotranspiration in semiarid grassland and shrubland ecosystems using time series of soil surface temperature, *Agric. For. Meteorol.*, *149*, 59–72.
Newman, B. D., B. P. Wilcox, S. Archer, D. D. Breshears, C. N. Dahm, C. J. Duffy, N. G. McDowell, F. M. Phillips, B. R. Scanlon, and E. R. Vivoni (2006), The ecohydrology of arid and semiarid environments: A scientific vision, *Water Resour. Res.*, *42*, W06302, doi:10.1029/2005WR004141.
Peel, M. C., B. L. Finlayson, and T. A. McMahon (2007), Updated world map of the Köppen-Geiger climate classification, *Hydrol. Earth Syst. Sci.*, *11*, 1633–1644.

Pereira, F. L., J. H. C. Gash, J. S. David, T. S. David, P. R. Monteiro, and F. Valente (2009), Modelling interception loss from evergreen oak Mediterranean savannas: Application of a tree-based modelling approach, *Agric. For. Meteorol.*, *149*(3–4), 680–688.
Pitman, J. I. (1989), Rainfall interception by bracken in open habitats relations between leaf area, canopy storage and drainage rate, *J. Hydrol.*, *105*, 317–334.
Privette, J. L., R. B. Myneni, Y. Knyazikhin, M. Mukelabai, and G. Roberts (2002), Early spatial and temporal validation of MODIS LAI product in the Southern Africa Kalahari, *Remote Sens. Environ.*, *83*, 232–243.
Rawls, W. J., and D. L. Brakensiek (1989), Estimation of soil water retention and hydraulic properties, in *Unsaturated Flow in Hydrologic Modeling: Theory and Practice*, pp. 275–300, Kluwer Acad., Dordrecht, Netherlands.
Rawls, W. J., D. L. Brakensiek, and N. Miller (1983), Green-Ampt infiltration parameters from soils data, *J. Hydraul. Eng.*, *109*(1), 62–70.
Raz-Yaseef, N., D. Yakir, G. Schiller, and S. Cohen (2012), Dynamics of evapotranspiration partitioning in a semi-arid forest as affected by temporal rainfall patterns, *Agric. For. Meteorol.*, *157*, 77–85.
Reynolds, J. F., P. R. Kemp, and J. D. Tenhunen (2000), Effects of long-term rainfall variability on evapotranspiration and soil water distribution in the Chihuahuan Desert: A modeling analysis, *Plant Ecol.*, *150*, 145–159.
Robles-Morua, A., E. R. Vivoni, and A. Mayer (2012), Distributed hydrologic modeling in Northwest Mexico reveals the links between runoff mechanisms and evapotranspiration, *J. Hydrometeorol.*, *13*, 785–807.
Rodríguez-Iturbe, I., A. Porporato, F. Laio, and L. Ridolfi (2001), Intensive versus extensive use of soil moisture: Plant strategies to cope with stochastic water availability, *Geophys. Res. Lett.*, *28*, 4495–4497.
Rutter, A. J., K. A. Kershaw, P. C. Robins, and A. J. Morton (1971), A predictive model of rainfall interception in forests. 1: Derivation of the model from observation in a plantation of Corsican pine, *Agric. Meteorol.*, *9*, 367–384.
Ryu, Y., J. Verfaille, C. Macfarlane, H. Kobayashi, O. Sonnentag, R. Vargas, S. Ma, and D. Baldocchi (2012), Continuous observations of tree leaf area index at ecosystem scale using upward-pointing digital cameras, *Remote Sens. Environ.*, *126*, 115–125.
Schulze, E. D., R. Leuning, and F. M. Kelliher (1995), Environmental regulation of surface conductance for evaporation from vegetation, *Vegetatio*, *121*, 79–87.
Scott, R. L., E. A. Edwards, W. J. Shuttleworth, T. E. Huxman, C. J. Watts, and D. C. Goodrich (2004), Interannual and seasonal variations in fluxes of water and carbon dioxide from a riparian woodland ecosystem, *Agric. For. Meteorol.*, *122*, 64–84.
Scott, R. L., T. E. Huxman, W. L. Cable, and W. E. Emmerich (2006), Partitioning of evapotranspiration and its relation to carbon dioxide exchange in a Chihuahuan desert shrubland, *Hydrol. Processes*, *20*, 3227–3243.
Seyfried, M. S., and M. D. Murdock (2004), Measurement of soil water content with a 50-MHz soil dielectric sensor, *Soil Sci. Soc. Am. J.*, *68*, 394–403.
Shuttleworth, W. J. (1992), Evaporation, in *Handbook of Hydrology*, edited by D. R. Maidment, pp. 4.11–4.18, McGraw-Hill, New York.
Stannard, D. I., and M. A. Weltz (2006), Partitioning evapotranspiration in sparsely vegetated rangeland using a portable chamber, *Water Resour. Res.*, *42*, W02413, doi:10.1029/2005WR004251.
Sugiyama, S., M. Yoneyama, N. Takahashi, and K. Gotoh (1985), Canopy structure and productivity of Festuca arundinacea Schreb, during vegetative and reproductive growth, *Grass Forage Sci.*, *40*, 49–55.
Tang, Q., E. R. Vivoni, F. Munoz-Arriola, and D. P. Lettenmaier (2012), Predictability of evapotranspiration patterns using remotely-sensed vegetation dynamics during the North American monsoon, *J. Hydrometeorol.*, *13*, 103–121.
Tarín, T. T., E. A. Yépez, J. Garatuza-Payán, C. J. Watts, J. C. Rodríguez, E. R. Vivoni, and L. A. Méndez-Barroso (2014), Evapotranspiration partitioning with stable isotopes in ecohydrological studies, *Water Technol. Sci.*, *5*(3), in press.
Van den Hurk, B. J. J. M., P. Viterbo, and S. O. Los (2003), Impact of leaf area index seasonality on the annual land surface evaporation in a global circulation model, *J. Geophys. Res.*, *108*(D6), 4191, doi:10.1029/2002JD002846.
Van Genuchten, M. T. (1980), Predicting the hydraulic conductivity of unsaturated soil, *Soil Sci. Soc. Am. J.*, *44*, 892–898.
Vargas, R., et al. (2013), Progress and opportunities for monitoring greenhouse gases fluxes in Mexican ecosystems: The MexFlux Network, *Atmósfera*, *26*(3), 325–336.
Vivoni, E. R. (2012), Diagnosing seasonal vegetation impacts on evapotranspiration and its partitioning at the catchment scale during SMEX04-NAME, *J. Hydrometeorol.*, *13*, 1631–1638.
Vivoni, E. R., D. Entekhabi, R. L. Bras, and V. Y. Ivanov (2007a), Controls on runoff generation and scale-dependence in a distributed hydrologic model, *Hydrol. Earth Syst. Sci.*, *11*(5), 1683–1701.
Vivoni, E. R., et al. (2007b), Variation of hydrometeorological conditions along a topographic transect in northwestern Mexico during the North American monsoon, *J. Clim.*, *20*(9), 1792–1809.
Vivoni, E. R., H. A. Moreno, G. Mascaro, J. C. Rodríguez, C. J. Watts, J. Garatuza-Payán, and R. L. Scott (2008), Observed relation between evapotranspiration and soil moisture in the North American monsoon region, *Geophys. Res. Lett.*, *35*, L22403, doi:10.1029/2008GL036001.
Vivoni, E. R., J. C. Rodríguez, and C. J. Watts (2010), On the spatiotemporal variability of soil moisture and evapotranspiration in a mountainous basin within the North American monsoon region, *Water Resour. Res.*, *46*, W02509, doi:10.1029/2009WR008240.
Watts, C. J., R. L. Scott, J. Garatuza-Payán, J. C. Rodríguez, J. H. Prueger, W. P. Kustas, and M. Douglas (2007), Changes in vegetation condition and surface fluxes during NAME 2004, *J. Clim.*, *20*, 1810–1820.
Webb, E. K., G. I. Pearman, and R. Leuning (1980), Correction of flux measurements for density effects due to heat and water vapour transfer, *Q. J. R. Meteorol. Soc.*, *106*, 85–100.
Wigmosta, M. S., L. Vail, and D. P. Lettenmaier (1994), A distributed hydrology-vegetation model for complex terrain, *Water Resour. Res.*, *30*, 1665–1679.
Wilczak, J. M., S. P. Oncley, and S. A. Stage (2001), Sonic anemometer tilt correction algorithms. *Boundary Layer Meteorol.*, *99*, 127–150.
Wilson, J. L., and H. Guan (2004), Mountain-block hydrology and mountain front recharge, in *Groundwater Recharge in a Desert Environment: The Southwestern United States, Water Science and Applications*, vol. 9, pp. 113–137, AGU, Washington, D. C.
Wilson, K., A. Goldstein, E. Falge, M. Aubinet, and D. Baldocchi (2002), Energy balance closure at FLUXNET sites, *Agric. For. Meteorol.*, *113*, 223–243.
Yan, H., et al. (2012), Global estimation of evapotranspiration using a leaf area index-based surface energy and water balance model, *Remote Sens. Environ.*, *124*, 581–595.
Yang, Y., R. L. Scott, and S. Shang (2013), Modeling evaporation and its partitioning over a semiarid shrub ecosystem from satellite imagery: A multiple validation, *J. Appl. Remote Sens.*, *7*, 073495, doi:10.1117/1.JRS.7.073495.
Yépez, E. A., D. Williams, R. Scott, and G. Lin (2003), Partitioning overstory and understory evapotranspiration in a semiarid savanna woodland from the isotopic composition of water vapor, *Agric. For. Meteorol.*, *119*, 53–68.
Yépez, E., R. Scott, W. Cable, and D. Williams (2007), Intraseasonal variation in water and carbon dioxide flux components in a semiarid riparian woodland, *Ecosystems*, *10*, 1100–1115.